THE JOURNAL OF BIOLOGICAL CHEMISTRY VOL. 289, NO. 9, pp. 5635–5653, February 28, 2014

Functional Cross-talk between Distant Domains of Chikungunya Virus Non-structural Protein 2 Is Decisive for Its RNA-modulating Activity*

Received for publication, July 18, 2013, and in revised form, December 16, 2013 Published, JBC Papers in Press, January 9, 2014, DOI 10.1074/jbc.M113.503433

Pratyush Kumar Das[1], **Andres Merits**[2], **and Aleksei Lulla**[3]

From the Institute of Technology, University of Tartu, Nooruse 1, 50411 Tartu, Estonia

Background: RNA helicase activity of chikungunya virus (CHIKV) non-structural protein 2 (nsP2) has not been previously demonstrated.
Results: CHIKV nsP2 possesses 5′–3′ RNA helicase and RNA annealing activities.
Conclusion: RNA-modulating activities of nsP2 apparently depend on communication between N-terminal and C-terminal domains of nsP2.
Significance: Optimization of RNA helicase assay for nsP2 of highly medically important CHIKV opens opportunities for inhibitor screening studies.

Chikungunya virus (CHIKV) non-structural protein 2 (nsP2) is a multifunctional protein that is considered a master regulator of the viral life cycle and a main viral factor responsible for cytopathic effects and subversion of antiviral defense. The C-terminal part of nsP2 possesses protease activity, whereas the N-terminal part exhibits NTPase and RNA triphosphatase activity and is proposed to have helicase activity. Bioinformatics analysis classified CHIKV nsP2 into helicase superfamily 1. However, the biochemical significance of a coexistence of two functionally unrelated modules in this single protein remains unknown. In this study, recombinant nsP2 demonstrated unwinding of double-stranded RNA in a 5′–3′ directionally biased manner and RNA strand annealing activity. Comparative analysis of NTPase and helicase activities of wild type nsP2 with enzymatic capabilities of different truncated or N-terminally extended variants of nsP2 revealed that the C-terminal part of the protein is indispensable for helicase functionality and presumably provides a platform for RNA binding, whereas the N-terminal-most region is apparently involved in obtaining a conformation of nsP2 that allows for its maximal enzymatic activities. The establishment of the protocols for the production of biochemically active CHIKV nsP2 and optimization of the parameters for helicase and NTPase assays are expected to provide the starting point for a further search of possibilities for therapeutic interventions to suppress alphaviral infections.

Chikungunya virus (CHIKV)[4] is an important, recently reemerged human pathogen causing acute illness associated with fever, skin rash, and arthralgia (1). CHIKV belongs to the Semliki Forest virus (SFV) serological complex within the *Alphavirus* genus of the Togaviridae family (2). The positive-strand RNA genome of CHIKV is ~11.8 kb in length and exhibits a 5′-terminal methylguanylate cap-0 structure and a 3′ poly(A) sequence (3). Viral genome replication is carried out by the non-structural (ns) proteins that are initially produced as part of ns polyproteins P123 and P1234, which are later sequentially cleaved by the viral protease residing in the nsP2 region to ultimately generate mature nsP1, nsP2, nsP3, and nsP4 (4, 5). The ns polyproteins, their cleavage intermediates, and mature nsPs are multifunctional, displaying different enzymatic activities and representing indispensable virus-encoded components of replication complexes. Alphaviral nsP1 mediates membrane binding (6) and possesses methyltransferase and guanylyltransferase activities that are used for capping viral positive-strand RNAs (7, 8). NsP2 contributes to the capping process through its RNA triphosphatase activity (9) and possesses experimentally demonstrated NTPase (10, 11) and protease functionalities (12, 13) along with previously insufficiently studied helicase activity (14). NsP3 contains a macrodomain that shows affinity toward poly(ADP-ribose) and RNA (15), a zinc-binding domain (16), and a hypervariable C-terminal region involved in virus adaptation to the host (17). NsP4 is a viral RNA-dependent RNA polymerase (18).

In infected cells, nsP2 localizes to both the cytoplasm and the nucleus (19) where it displays multiple activities, including inducing the cessation of cellular transcription and inhibiting antiviral responses (20, 21). Bioinformatics analysis suggests that alphaviral nsP2 comprises five domains (see Fig. 1*A*): an

* This work was supported in part by Estonian Science Foundation Grant 9421, Targeted Financing Project SF0180087s08, the European Union 7th Framework *Integrated Chikungunya Research* project, and the European Union through the European Regional Development Fund via the Center of Excellence in Chemical Biology.
[1] Recipient of a scholarship from the European Union Social Fund via Activity 4 of the Doctoral Studies and Internationalisation Programme.
[2] To whom correspondence may be addressed. Tel.: 372-737-5007; Fax: 372-737-4900; E-mail: andres.merits@ut.ee.
[3] To whom correspondence may be addressed. Tel.: 372-737-5007; Fax: 372-737-4900; E-mail: aleksei.lulla@ut.ee.

[4] The abbreviations used are: CHIKV, Chikungunya virus; aa, amino acid(s); ns, non-structural; nsP, non-structural protein; SFV, Semliki Forest virus; SF, superfamily; NTP, nucleoside triphosphate; RI, replicative intermediate; ds, double-stranded; ss, single-stranded; TEV, tobacco etch virus; ToMV, tomato mosaic virus; NTD, N-terminal domain; MTL, methyltransferase-like; Ni-TED, nickel-*tris(carboxymethyl)ethylene diamine; Hel, helicase*.

N-terminal domain (NTD; amino acids (aa) ~1–167; no known analogs outside of *Alphavirus* genus), two RecA-like domains (aa ~168–470) presumably capable of NTP hydrolysis, a papain-like protease domain (aa ~471–605), and an Ftsj methyltransferase-like (MTL) domain (aa ~606–798) that is apparently non-functional as a methyltransferase because of the absence of a number of crucial structural elements. Four known enzymatic activities of nsP2 are associated with different regions of the protein: its C-terminal part, involving the protease and MTL domains (aa 471–798), exhibits protease activity, whereas the N-terminal part (aa 1–470) displays NTPase and RNA triphosphatase activities and is evidently important for RNA helicase activity. The protease (22), NTPase, and RNA triphosphatase activities (11) have been experimentally confirmed for different protein fragments derived from CHIKV nsP2, whereas its RNA helicase activity has not yet been experimentally demonstrated.

Helicases are motor proteins that utilize energy derived from the hydrolysis of NTPs or dNTPs to unwind double-stranded (ds) nucleic acids into their component single strands. More broadly, these proteins represent a subset of "translocases" that also move along nucleic acids without unwinding them. Helicases are classified into six superfamilies (SFs) among which enzymes belonging to SF1 and SF2 are monomeric, whereas enzymes from other SFs act as oligomeric proteins (23). The alphaviral nsP2 helicase belongs to SF1 (24). Helicases from SF1 and SF2 usually contain two RecA-like domains that participate in the binding and hydrolysis of NTP or dNTP molecules (25). These RecA-like domains contain seven classical motifs based on which helicase classification was initially conducted. Of these motifs, Walker A (motif I), Walker B (motif II), and the arginine finger (motif VI) are considered to be the core motifs (23). In addition, accessory domains that do not directly contribute to NTP binding or hydrolysis may have a particular importance for helicase functioning (26). For several SF2 helicases, it has been shown that these domains play a critical role by interacting with nucleic acids (27–29).

Of all alphaviruses, the helicase functionality has been demonstrated only for SFV nsP2. The enzyme activity was found to be rather weak, and the direction of dsRNA unwinding has not been revealed. RNA helicase activity of SFV nsP2 was shown using a purified recombinant protein with 17 non-native aa residues (including a hexahistidine (His_6) affinity tag) attached to its N terminus (14). However, other studies demonstrated that the specific sequence at the N terminus of nsP2 is an important factor or even an absolute requirement for several activities of the protein, including the induction of major cytotoxic effects in vertebrate cells (20) and the processing of the cleavage site between nsP2 and nsP3 (30). Therefore, the possibility that an N-terminal affinity tag could compromise or alter the RNA helicase activity of this enzyme cannot be excluded. Furthermore, because alphavirus nsP2 belongs to the SF1 helicases, it is expected to exhibit high basal NTPase activity (31). However, to date, the NTPase activities determined experimentally for purified recombinant nsP2 proteins have been moderate or low (9–11), which may possibly be related to their insufficient nativeness and purity. This assumption is bolstered by the speculation that several aa residues located upstream of the intact N terminus of nsP2 may hinder the protein from folding into its most native conformation (10). Finally, it has been shown that a recombinant form of CHIKV nsP2 lacking 166 aa residues at its N terminus and 168 aa residues at its C terminus exhibits NTPase and RNA triphosphatase activities but still completely lacks RNA helicase activity (11), which suggests that the regions located at the N and/or C terminus of nsP2 may be important for this activity.

In this study, we characterized the NTPase, RNA helicase, and RNA-annealing activities of CHIKV nsP2. A bioinformatics approach was applied in an attempt to understand the possible folding pattern of the N-terminal region of nsP2 (N470; aa 1–470), which was suggested to possess helicase activity, and to identify key aa residues that may interact with NTP or dNTP molecules. Furthermore, the purification techniques standardized in this study may be used as a platform to purify native and highly functional nsP2 for structural studies. The enzymatic assays developed and applied in this work also represent potential tools for the screening of antiviral molecules that may be capable of inhibiting CHIKV infection.

EXPERIMENTAL PROCEDURES

Three-dimensional Structural Modeling of CHIKV N470—The sequence of the N-terminal region encompassing aa 1–470 of CHIKV (LR2006-OPY1 strain) nsP2 was processed using the Protein Homology/Analogy Recognition Engine (PHYRE) and PHYRE 2 (32), I-TASSER (33), and MODELLER (34). The obtained structural model was manually compared with the published three-dimensional structures of SF1 helicases to identify the key aa residues. The PyMOL Molecular Graphics System (version 1.6.0.0, Schrödinger, LLC) was used to exploit the various aspects of the modeled structure (35).

Molecular Cloning and Site-directed Mutagenesis—The sequence encoding CHIKV nsP2 was codon-optimized (Invitrogen) for the *Escherichia coli* expression system, and the ultimate Cys-798 was changed to Ala in all constructs. Conventional cloning and PCR-based techniques were used to generate the required protein expression constructs using the pET-28a vector (Merck Millipore) as a backbone. pET-nsP2 encoded MNHHHHHHSGG-(thioredoxin)-GSSSG-LDRAGG ↓ nsP2, in which the CHIKV nsP2 sequence, preceded by the nsP3 part (LDRAGG) of the hybrid nsP3/nsP2 cleavage site and flexible linker region, was fused to a His_6 purification tag and thioredoxin domain. This type of hybrid substrate has been observed to be better processed than the natural nsP1/nsP2 protease substrate in the case of SFV (30, 36). pET-His-nsP2 encoded CHIKV nsP2 preceded by aa sequence MNHHHHHH-SGGGS-ENLYFQ, which contained a His_6 tag and tobacco etch virus (TEV) protease cleavage site separated by a flexible linker. pET-N470 encoded N470, the N-terminal fragment of nsP2 encompassing aa 1–470, fused to the MNHHHHHHSGGGSENLYFQ sequence as indicated above. Expression vectors designated pET-N470-K192A, pET-N470-D252A, and pET-N470-E253A, containing mutations resulting in the specified aa substitutions in N470, were generated via PCR-based site-directed mutagenesis. Similarly, a PCR-based mutagenesis approach was utilized to generate the constructs for expression of the modified versions of nsP2 (see Fig. 1*A*). To this end, nsP2-delN2 (deletion of aa 1–2 at the N

terminus of nsP2) and nsP2-insN2 (addition of GA dipeptide to the N terminus of nsP2) were made using pET-nsP2 as a template, whereas nsP2-delNTD (deletion of aa 1–167) and nsP2-delMTL (deletion of aa 606–798) were made on the basis of pET-His-nsP2. The sequences of all the expression constructs were verified through DNA sequencing. The details of the cloning procedures and the sequences of the obtained constructs are available from the authors upon request.

Expression and Purification of N470 Proteins—An adapted autoinduction protocol was used for recombinant protein expression (37). Briefly, *E. coli* BL21(DE3) cells (Merck Millipore) transformed with pET-N470 were grown to an A_{600} of 0.8–1.0 at 37 °C with shaking at 250 rpm in 1 liter of Difco Terrific Broth medium (BD Biosciences) containing 0.8% glycerol and supplemented with kanamycin (50 μg/ml), 2 mM $MgSO_4$, 0.5% (w/v) lactose, and 0.015% (w/v) glucose. Protein expression was conducted at 23 °C with shaking at 150 rpm for an additional 16–18 h. The cells were harvested via centrifugation and resuspended in 40 ml of lysis buffer A (50 mM Na_2HPO_4, pH 8.0, 300 mM NaCl, 1 mM 2-mercaptoethanol, 5% glycerol, and 0.5 mM Pefabloc SC (Roche Applied Science)). Next, 10,000 units of DNase I was added to the sample, and the cells were lysed using an EmulsiFlex-C3 high pressure homogenizer (Avestin, Germany). The lysate was cleared by centrifugation at 48,000 $\times$ *g* for 30 min, and the obtained supernatant was loaded onto a gravity flow column packed with 4 g of Protino Ni-TED resin (Macherey-Nagel, Germany) pre-equilibrated with buffer B (50 mM Na_2HPO_4, pH 8.0, 300 mM NaCl, 1 mM 2-mercaptoethanol, and 5% glycerol). The column was washed with 6 column volumes of the same buffer, and the proteins were then eluted with buffer B supplemented with 250 mM imidazole.

Removal of the His_6 tag was performed using TEV protease (purified in house) at an approximate molar ratio of 1:10 (TEV: N470) at 4 °C overnight followed by imidazole removal using an ÄKTA Purifier 100 chromatography system (GE Healthcare) and a HiPrep 26/10 desalting column equilibrated with buffer B. The sample was next passed through the column packed with Protino Ni-TED resin again, and the fraction containing N470 without the affinity tag was dialyzed against buffer C (50 mM HEPES, pH 7.2, 50 mM NaCl, and 5% glycerol). The protein solution was loaded onto a HiTrap SP FF 1 ml cation exchange column (GE Healthcare) and was gradient-eluted with buffer C containing 1.5 M NaCl. L-Arginine and L-glutamic acid at a final concentration of 50 mM were added to the eluted protein solution to prevent precipitation (38). The peak fractions were combined, concentrated via ultrafiltration using Amicon Ultra-15 centrifugal filter units (Merck Millipore), and loaded onto a Superdex 200 10/300GL size exclusion column (GE Healthcare) pre-equilibrated with buffer D (50 mM HEPES, pH 7.2, 300 mM NaCl, 5% glycerol, 1 mM 2-mercaptoethanol, 50 mM L-arginine, and 50 mM L-glutamic acid). The concentrations of the eluted N470 and the other recombinant proteins were measured using a Bio-Rad protein assay and BSA standards (Bio-Rad). The purified protein solutions were finally aliquoted, flash frozen in liquid nitrogen, and stored at −80 °C. The expression and purification of N470-K192A, N470-D252A, and N470-E253A were conducted as described above except that buffers A and B were supplemented with 10% glycerol.

Expression and Purification of NsP2 Variants—The expression and purification of His-nsP2 were performed essentially as described above except that following imidazole elution His-nsP2 was dialyzed against buffer E (50 mM HEPES, pH 8.0, 50 mM NaCl, and 5% glycerol), loaded onto a HiTrap SP FF 1-ml cation exchange column, and gradient-eluted with buffer E containing 1.5 M NaCl. Mutant proteins nsP2-delNTD and nsP2-delMTL were purified analogously to what has been described above. The TEV protease-mediated tag removal step was also included as in the N470 purification procedure, whereas the ion exchange step was bypassed because of low protein yield.

To purify nsP2, the clarified lysate (obtained as described for N470) was incubated for 2 h at 4 °C to achieve autocatalytic removal of the N-terminal tag and then loaded onto the Protino Ni-TED column. Proteins were eluted from the column without imidazole in several ~15-ml volumes of buffer B. Both the flow-through and wash fractions were analyzed by SDS-PAGE, and the fractions containing nsP2 were combined. The subsequent purification steps were identical to the protocol used for the purification of His-nsP2. Proteins nsP2-delN2 and nsP2-insN2 were purified using the same procedure as for nsP2. The identities of all purified proteins were confirmed by mass spectrometry with special attention to the correctness of the N-terminal regions.

Far-UV Circular Dichroism (CD) Spectroscopy—Secondary structural composition of the native and various mutated versions of nsP2 was analyzed using a CD spectrometer (Chirascan Plus, Applied Photophysics, UK) in CD buffer containing 10 mM KH_2PO_4, pH 7.2 and 100 mM NaF with a 1-mm-path length quartz cuvette (Hellma Analytics, Germany). Mean spectra were derived from three independent acquisitions in the far-UV region, ranging from 185 to 260 nm with an interval of 1 nm at 20 °C for each individual protein, at a concentration of 0.1 mg/ml. The spectra for the negative control comprising only CD buffer obtained under identical conditions were subtracted from the initial measurements for the protein samples. The final CD spectra were processed to be expressed as mean residue ellipticity. CDNN software, based on the neural network theory (39), was further used to determine the approximate percentage of each type of secondary structure in the recombinant proteins.

NTPase Assays—NTPase assays were performed using the EnzChek® Phosphate Assay kit (Invitrogen) according to the manufacturer's protocol. Briefly, 50 μl of 20-fold reaction buffer (1 M Tris-HCl, pH 7.5, 20 mM $MgCl_2$, and 2 mM NaN_3) was mixed with 200 μl of the 2-amino-6-mercapto-7-methylpurine riboside substrate, 1 unit of purine nucleoside phosphorylase, and recombinant enzymes: 1 pmol of nsP2, 3 pmol of His-nsP2, or 23 pmol of N470. The samples were brought to a volume of 900 μl with distilled water and incubated at 22 °C for 10 min. Continuous spectrophotometric measurements were performed using a Helios UV-visible spectrophotometer (Thermo Fischer Scientific) at a wavelength of 360 nm immediately after the addition of 100 μl of 1 mM NTP or dNTP as substrate. The reaction was allowed to proceed for 7–10 min. Finally, the changes in the

TABLE 1

Sequences of the RNA oligonucleotides used in this study

The DNA oligonucleotides have the same sequences except that U is substituted with T.

	Length	Sequence (5′–3′)
	bases	
Oligo 1	16	CGCUGAUGUCGCCUGG
Oligo 2	28	CCAGGCGACAUCAGCGAAAAAAAAAAAA
Oligo 3	16	CCAGGCGACAUCAGCG
Oligo 4	22	AAAAAACCAGGCGACAUCAGCG
Oligo 5	28	AAAAAAAAAAAACCAGGCGACAUCAGCG
Oligo 6	40	AAAAAAAAAAAAAAAAAAAAAAAACCAGGCGACAUCAGCG
Oligo 7	28	CGCUGAUGUCGCCUGGAAAAAAAAAAAA
Oligo 8	18	AAAAAAAAAAAAAAAAAA
Oligo 9	18	UUUUUUUUUUUUUUUUUU
Oligo 10	18	CCCCCCCCCCCCCCCCCC
Oligo 11	18	GGGGGGGGGGGGGGGGGG

A/min were calculated from the change in the slope/min, and the specific activities of N470, His-nsP2, and nsP2 were calculated. For the GTPase stimulation assay, the reactions were carried out as above except that the final reaction volume was adjusted to 200 μl, and 18-base RNA or DNA homo-oligomers (Table 1) at 1.75 μM concentration were included in the reaction mixture.

Optimization of the Mg^{2+} concentration in the NTPase reaction was also conducted essentially as described above except that N470 was incubated in 50 mM Tris-HCl buffer, pH 7.5 with 0–10 mM $MgCl_2$ instead of commercial reaction buffer. The reaction was initiated by the addition of ATP to a concentration 0.5 mM; the final reaction volume was 200 μl.

Determination of K_m and K_{cat} for GTP Hydrolysis—To measure parameters related to enzyme kinetics, the GTPase reaction was performed with different concentrations (1–200 μM) of GTP substrate. The Mg^{2+} concentration in each reaction was maintained at 6-fold above the concentration of GTP. K_m, K_{cat}, and the enzyme efficiency (K_{cat}/K_m) were calculated using the double reciprocal Lineweaver-Burk plot and fit to the Michaelis-Menten hyperbolic plot using Microsoft Excel software.

Temperature Dependence of the GTPase Activity—The effect of the temperature on the GTPase activity was analyzed by mixing all the reaction components in a volume of 200 μl as described for the standard NTPase assay (see above) and incubating the reaction mixtures for 10 min at the indicated temperature (see Fig. 3*F*). The reaction was initiated by adding GTP to a final concentration of 100 μM, and continuous spectrophotometric measurements were carried out at room temperature for 1–2 min. As a control, the activity of the purine-nucleoside phosphorylase enzyme involved in the EnzChek Phosphate Assay kit (Invitrogen) was additionally tested at the indicated temperatures using only standard phosphate solution.

Preparation of dsRNA and dsDNA Substrates—Preparation of the substrates for the helicase assays was performed as described previously (40). DNA and RNA oligonucleotides with the required sequences (Table 1) (adapted from Ref. 41) were obtained from Microsynth AG (Switzerland) and Exiqon (Denmark), respectively. Either both or one of the oligonucleotides (in the case of RNA substrates) or only oligonucleotide 1 (in the case of DNA substrates; Table 1) was labeled with ^{33}P at the 5′ terminus using [γ-^{33}P]ATP (PerkinElmer Life Sciences) and phage T4 polynucleotide kinase (Thermo Fisher Scientific). Oligonucleotides 1 and 2 were used to prepare substrates with a 12-base 3′ overhang, oligonucleotides 1 and 3 were used to prepare substrates with blunt ends, oligonucleotides 1 and 4 were used to prepare substrates with a 6-base 5′ overhang, oligonucleotides 1 and 5 were used to prepare substrates with a 12-base 5′ overhang, and oligonucleotides 1 and 6 were used to prepare substrates with a 24-base 5′ overhang. Oligonucleotides 5 and 7 were used to obtain a fork substrate with both 12-base 5′ and 3′ overhangs at one end. The mixtures were prepared in a final volume of 15 μl of buffer containing 10 mM HEPES, pH 7.2 and 20 mM KCl; heated to 95 °C; and allowed to slowly cool to 22 °C. The appropriate volume of 5-fold nondenaturing loading buffer containing 50% glycerol, 0.1% bromphenol blue, and 0.1% xylene cyanol was added, and the samples were resolved by 15% native PAGE. Radioactive dsRNA or dsDNA products were detected via brief exposure of the gel to x-ray film. The corresponding bands were cut out, and the gel was crushed after which nucleic acids were eluted through overnight incubation at 4 °C with buffer containing 300 mM sodium acetate, pH 5.4, 1 mM EDTA, and 0.5% SDS. The probes were centrifuged at 6000 × *g* for 5 min, and 2 μl of 50% glycerol and 3 volumes of 95% chilled ethanol were added to the obtained supernatant. The samples were incubated at −20 °C for 1 h, and the nucleic acids were precipitated via centrifugation at 4 °C at 12,000 × *g* for 30 min. The dsRNA or dsDNA probes were dissolved in 15 μl of buffer containing 10 mM HEPES, pH 7.2 and 20 mM KCl and then stored at −20 °C. The concentrations of the labeled dsRNA or dsDNA were estimated by measuring the radioactivity of a small aliquot of substrates using a Tri-Carb 2810TR liquid scintillation counter (PerkinElmer Life Sciences).

DNA and RNA Helicase Assays—In standard helicase assays, unless otherwise stated, 50 pM labeled dsRNA or 50 pM labeled dsDNA as a substrate was incubated with 12.5 nM recombinant enzymes in a buffer containing 20 mM HEPES, pH 7.2, 2 mM DTT, and 10 mM NaCl. In the experiments designed for the determination of the dependence of dsRNA unwinding based on the concentration of enzyme, the concentration of recombinant protein varied from 0.5 to 50 nM. The reaction volume was 15 μl, and a 20-min preincubation was performed at 22 °C. The reaction mixtures were subsequently split equally into three tubes, ATP and magnesium acetate in complex (ATP-Mg^{2+}) were added to a final concentration of 3.5 mM to one tube. In the other tubes, the same volume of nuclease-free water

was added. After 2 h of incubation at 37 °C, the reaction was terminated by the addition of an equal volume of stop buffer containing 50 mM EDTA, 1% SDS, 0.1% bromphenol blue, 0.1% xylene cyanol, and 20% glycerol. The substrate and reaction products were separated via 15% native PAGE. The gel was dried, exposed to a storage phosphor screen, and visualized using a Typhoon Trio scanner (GE Healthcare). The radioactivity corresponding to each band was quantified using NIH ImageJ software.

For the analysis of the time course of the helicase reaction, the assay was performed in a total volume of 60 μl. The composition of the reaction mixture and its preparation were the same as described above. A 5-μl aliquot was collected prior to the addition of 3.5 mM ATP-Mg^{2+} and 5 nM trap oligonucleotide 3 (Table 1). The RNA oligonucleotide was used as a trap except in the case of the 24-base 5′ overhang substrate where it was replaced with the DNA oligonucleotide, which provided the best reaction amplitude and consistent results. Subsequently, 5-μl aliquots of the reaction mixtures were collected at selected time points, and each aliquot was mixed with stop buffer and analyzed as described above.

Temperature Dependence of the RNA Helicase Activity—The effect of the temperature on the RNA helicase activity was analyzed in reactions containing 50 pM dsRNA with 12-base 5′ overhang as substrate, 12.5 nM enzyme, and 3.5 mM ATP-Mg^{2+} in a standard helicase assay buffer (see above). Briefly, the reaction was incubated at 22 °C for 20 min, then ATP-Mg^{2+} complex was added to a final concentration of 3.5 mM, and the reaction tubes were transferred to a thermostat with the indicated temperature (see Fig. 7*E*) and incubated for an additional 2 h. The products were resolved on a native gel and processed as described above.

RNA Annealing Assay—RNA annealing reactions were performed at 22 °C in 60 μl of a reaction mixture containing 20 mM HEPES, pH 7.2, 2 mM DTT, 0.5 mM Mg^{2+}, 1 mM NaCl, and 12.5 nM enzyme without ATP. Next, various dsRNA substrates (see Fig. 6) at 50 pM concentration were denatured for 2 min at 95 °C and then chilled on ice for 1 min before being added to the reaction mixture. Finally, 5-μl aliquots of the reaction mixtures were collected at selected time points and analyzed as described above.

RESULTS

Three-dimensional Structural Modeling of CHIKV N470—The three-dimensional structure of the fragment corresponding to the C-terminal part of CHIKV nsP2 (aa 471–791) has been previously resolved at 2.4-Å resolution (Protein Data Bank code 3TRK), revealing a fold highly similar to that of nsP2 protease from Venezuelan equine encephalitis virus (Protein Data Bank code 2HWK (43)). The three-dimensional structure of the remaining segment of nsP2 is still not known. Therefore, a homology modeling approach was used to predict the folding pattern of N470 using the I-TASSER (33), MODELLER (34), and PHYRE 2 and PHYRE (32) on-line servers. The first three servers identified the structure of the fragment covering aa 666–1116 of tomato mosaic virus (ToMV; a member of the alphavirus-like superfamily of positive-strand RNA viruses) replication protein predicted to have signatures of SF1 helicase (ToMV-Hel; Protein Data Bank code 3VKW (44)) as the best template for prediction of the folding of N470. The best model proposed by the PHYRE server was based on the structure of Upf1 helicase (Protein Data Bank code 2GJK (45)). The Upf1-based model covered only aa 46–444 of CHIKV nsP2, whereas the ToMV-based model covered aa 1–470, and it was selected to represent the possible structure of the N-terminal part of nsP2 (Fig. 1*B*, *left panel*). The model predicted the folding of N470 into three distinct domains with high overall similarity to the folding of ToMV-Hel (Fig. 1*B*, *right panel*). All of the known SF1 and SF2 helicases contain RecA-like domains, which are composed of a number of β-strands flanked by α-helices (46, 47). Two of these domains (domains 1A and 2A) were predicted to exist in N470, whereas the NTD was mostly presented as a disordered region (Fig. 1*B*, *left panel*). In contrast to Upf1 helicase, which contains accessory insertion domains 1B and 1C that have been reported to coordinate the nucleotide binding and RNA affinity of the protein (45), such domains were not found in the structure of ToMV-Hel (44) or in the model of N470 built on its basis (Fig. 1*B*).

The comparative analysis of the predicted structural model of N470 along with the examination of the aligned sequences representing homologous nsP2 regions from different alphaviruses allowed deduction of the motifs typically found in RecA-like domains (Fig. 1*C*). The aa residues were predicted based on their likeliness to interact with Mg^{2+}, nucleobase, ribose ring, and γ- and β-phosphate groups. These aa residues, which are conserved for all alphaviruses (Fig. 1*C*), were distributed across the classical motifs of RecA-like domains at positions similar to the motifs found in the three-dimensional structures of Upf1 (45), PcrA (26), and ToMV-Hel (44) helicases. Table 2 summarizes the results of this analysis. Briefly, the Walker A motif (motif I) contained the conserved residue Lys-192, which supposedly interacts with γ-phosphate; Asp-252 and Glu-253, the residues found in the Walker B motif (motif II), are presumed to interact with the Mg^{2+} and water molecules, respectively (48). Arg-416 that may also interact with γ-phosphate was located in the predicted arginine finger motif (motif VI) (Table 2). However, we were unable to identify a classical nucleobase-binding pocket in our three-dimensional model, which indicates that this pocket may be flexible in nsP2. This flexibility may occur because nsP2 as an RNA triphosphatase is expected to accommodate not only NTP but also RNA substrates.

Production of Recombinant Enzymes—The N-terminal Gly residue of nsP2 originates from the proteolytic cleavage of the polyprotein precursor. Notably, any extra or missing aa residues were previously found to strongly diminish the ability of nsP2 to cleave the site between nsP2 and nsP3 in the case of SFV (30). An analogous strict dependence on the identity of the N-terminal aa residue was observed for the RNA-dependent RNA polymerase activity of alphaviral nsP4 (49). Thus, to reveal the true functionalities of individual ns proteins of alphaviruses, their N termini should preferably remain intact. On the other hand, using tags for protein purification purposes provides clear advantages of simpler procedures needed to isolate the enzyme of interest, but often the tags remain attached to the protein as they are assumed to be neutral for enzymatic activity measurements. To illustrate the importance of the above con-

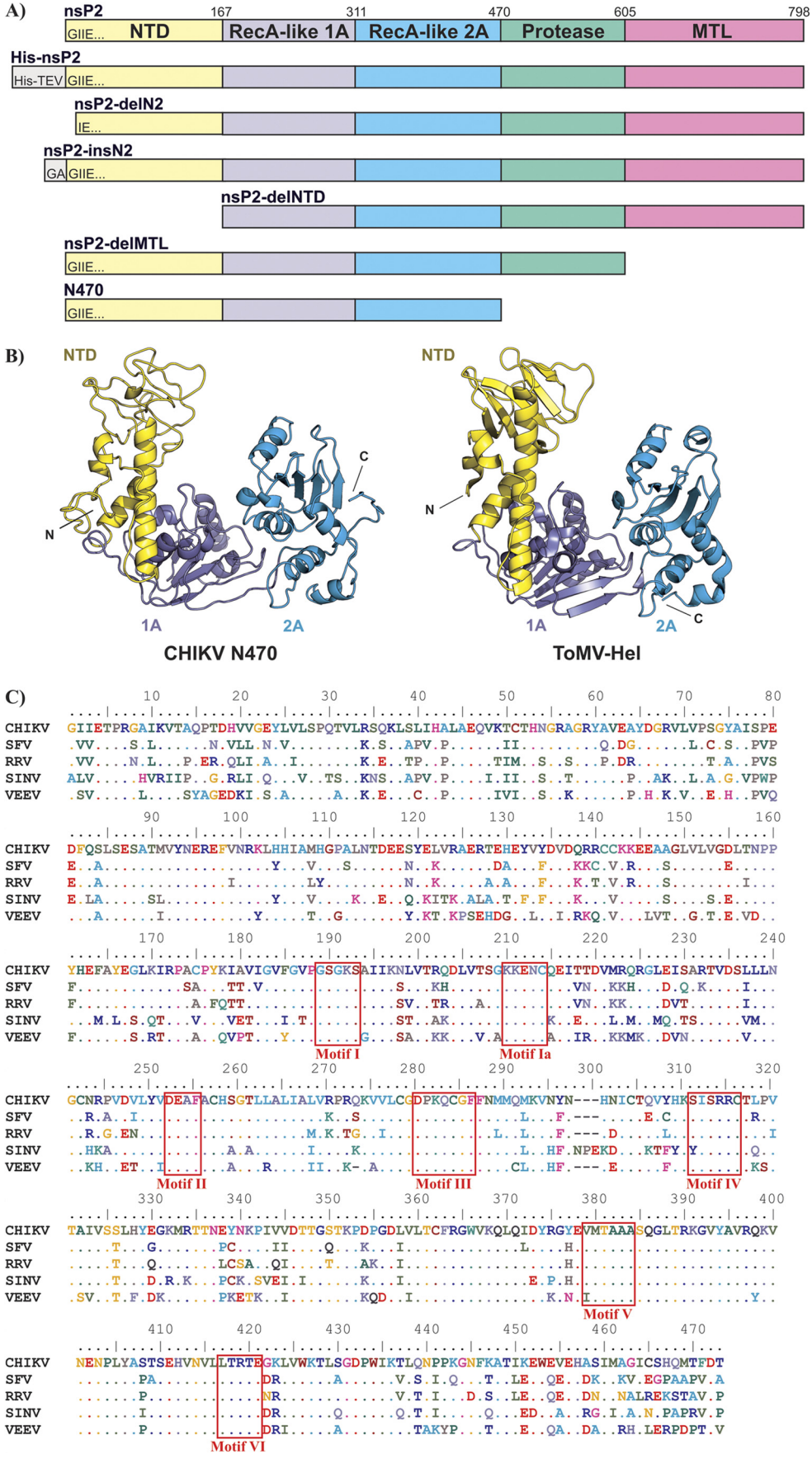
A)
nsP2
167
311
470
605
798
GIIE...
NTD
RecA-like 1A
RecA-like 2A
Protease
MTL
His-nsP2
His-TEV
nsP2-delN2
IE...
nsP2-insN2
GA
nsP2-delNTD
nsP2-delMTL
N470
B)
NTD
N
C
1A
2A
CHIKV N470
ToMV-Hel
C)
CHIKV
SFV
RRV
SINV
VEEV
Motif I
Motif Ia
Motif II
Motif III
Motif IV
Motif V
Motif VI

TABLE 2

Comparison of aa residues demonstrated (Upf1 and PcrA) or predicted (ToMV-Hel and N470) to interact with different moieties of the NTP molecule, incoming water molecules, and Mg^{2+} cations

The numbers of corresponding conserved motifs are shown in parentheses.

Interacting partner	Upf1 (45)	PcrA (26)	ToMV-Hel (44)	CHIKV N470 (this study)
Mg^{2+}	Asp-636 (II)	Asp-223 (II)	Asp-906 (II)	Asp-252 (II)
Water molecule	Glu-637 (II)	Glu-224 (II)	Glu-907 (II)	Glu-253 (II)
Nucleobase pocket	Tyr-702 (IV)	Tyr-286 (IV)	Leu-967 (IV)	Arg-311 (IV)
Ribose ring	Val-500 (I)	Arg-39 (I)	Lys-841 (I)	Ala-194 (I)
γ-Phosphate	Lys-498 (I)	Lys-37[a] (I)	Lys-839 (I)	Lys-192 (I)
	Gln-665 (III)	Gln-254 (III)	Gln-936 (III)	Gln-283 (III)
	Arg-703 (IV)	Arg-287 (IV)	Arg-968 (IV)	Arg-312 (IV)
	Arg-865 (VI)	Arg-610 (VI)	Arg-1076 (VI)	Arg-416 (VI)

[a] Interacts with β-phosphate.

siderations, a head-to-head comparison of the properties of the N-terminally tagged recombinant protein (His-nsP2) and the protein with an authentic N terminus (nsP2) was performed throughout this study.

Initial attempts to express N470 in fusion with the small ubiquitin-like modifier domain, which is known to improve fusion protein solubility (50), were unsuccessful: the expressed recombinant protein was rapidly degraded, which may have been the result of steric clashes between small ubiquitin-like modifier and N470 subdomains. Therefore, N470 was expressed in the form of a His_6-tagged fusion protein, which upon cleavage with TEV protease yielded a protein with an authentic N-terminal Gly residue. This approach resulted in high yields of recombinant protein in which no contaminants were detected by SDS-PAGE analysis (Fig. 2*A*, *lane 1*). The yields of N470-K192A, N470-D252A, and N470-E253A containing mutations in motifs I and II (Table 2) were reproducibly 4–6-fold lower than the yield of N470. Nevertheless, the obtained purified proteins were soluble and essentially free of contaminants (data not shown).

Moderate binding conditions (51) were required to facilitate the binding of full-length nsP2 to the cation exchange column. Under these conditions, pure His-nsP2 (Fig. 2*A*, *lane 3*) was obtained. However, unlike what was observed for N470, the cleavage site in the N-terminal tag of His-nsP2 was completely inaccessible to TEV protease, most likely due to steric hindrance (52). Interestingly, in the case of the truncated versions of His-nsP2 in which either the NTD (aa 1–167) or MTL (aa 606–798) domain was deleted, the TEV protease cleavage sites at the N termini were easily accessible for the respective protease, allowing the removal of the affinity tag to obtain tagless purified proteins (Fig. 2*A*, *lanes 6* and *7*). These data imply that in the case of His-nsP2 the formation of specific contacts involving the N-terminal-most region and MTL domain of nsP2 possibly restricted TEV protease access. As an alternative approach to obtain nsP2 with a native N terminus, a segment of the protease cleavage site consisting of 6 aa residues representing the extreme C terminus of nsP3 was appended to the N terminus of nsP2. The introduced cleavage site sequence was efficiently recognized and cleaved by the protease activity of nsP2 itself. Application of this modified purification strategy resulted in pure nsP2 (Fig. 2*A*, *lane 2*). A similar approach was used for generation of the nsP2-insN2 and nsP2-delN2 mutants, bearing addition or deletion of 2 aa residues at the N terminus of nsP2, respectively (Fig. 2*A*, *lanes 4* and *5*).

NsP2 and Its Modified Versions Are Comparably Folded—The extent of the structural differences between wild type (WT) nsP2 and its various truncated, extended, or tagged versions was analyzed using CD spectroscopy. These spectra in the far-UV region suggested that the analyzed recombinant proteins were properly and comparably folded (Fig. 2*B*). α-Helices were dominant components, constituting almost 40–42% of the secondary structure elements; β-sheets contributed around 12% of the secondary structure, whereas nearly 24% of the structural elements were estimated to form random coils. The nsP2 variants with the deletion of NTD or MTL, both of which demonstrated formation of high molecular weight aggregates according to size exclusion chromatography profiles, exhibited CD spectra with abnormally high ellipticity (data not shown), which also indicates the formation of protein aggregates.

The C-terminal Region and N Terminus Have a Strong Impact on the NTPase Activity of Recombinant NsP2—Previously, the recombinant proteins representing different fragments from alphaviral nsP2s have been shown to exhibit NTP hydrolysis rate that is lower (Table 3) (9–11) than would be characteristic for SF1 helicases (31). To understand this discrepancy, different variants of nsP2 and N470 proteins were analyzed for their ability to hydrolyze eight canonical NTPs and dNTPs. As expected, N470, nsP2, and His-nsP2 hydrolyzed all eight substrates (Fig. 3*A*). However, N470-K192A, N470-D252A, and N470-E253A were completely inactive (data not shown). This finding confirms that the aa residues identified through bioinformatics analysis (Table 2) were indeed crucial for the NTPase activity of the protein. Therefore, these mutants of N470 were excluded from further assays.

FIGURE 1. *A*, schematic representation of the putative modular organization of the CHIKV nsP2 is shown on *top*; presumable interdomain linker regions are not shown. The outline of the constructs used in this study is presented *below* showing modifications introduced into the nsP2 with the emphasis on the alterations in the N-terminal region. *B*, comparison of the three-dimensional model of the N-terminal region of CHIKV nsP2 with the three-dimensional structure of the ToMV-Hel fragment (aa 666–1116 of ToMV replicase). The *left panel* represents the three-dimensional model of the region encompassing aa 1–470 of CHIKV nsP2 built by the I-TASSER server (33) using the three-dimensional structure of ToMV-Hel (Protein Data Bank code 3VKW (44)); *right panel*) as a template. In both structures, domains 1A and 2A represent the RecA-like domains. Although predicted as mostly disordered, the possible folding of NTD of CHIKV nsP2 appears to resemble that of the N-terminal domain of ToMV-Hel. *C*, comparison of the sequence encompassing aa residues 1–470 of CHIKV nsP2 with corresponding sequences from different alphaviruses. Seven classical helicase motifs are highlighted with *boxes*. SFV, Ross River virus (*RRV*), Sindbis virus (*SINV*) are Old World alphaviruses, and Venezuelan equine encephalitis virus (*VEEV*) is a New World alphavirus.

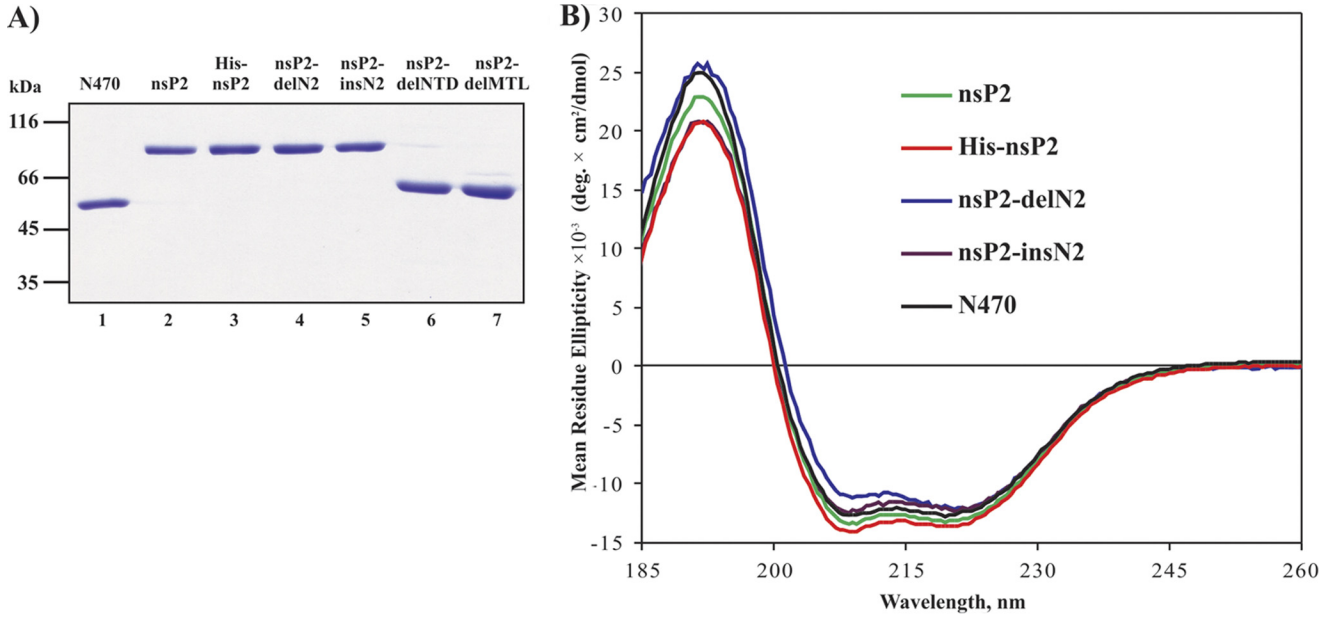

FIGURE 2. *A*, SDS-PAGE analysis of the purified recombinant proteins. Approximately 1 μg of each protein was analyzed by 10% SDS-PAGE, and the gel was stained with Coomassie Brilliant Blue. The positions of the molecular mass standards are shown at the *left* of the panel. *B*, CD spectroscopy analysis of the nsP2 and its modified variants. WT nsP2 and its various truncated, extended, or tagged versions were found to be properly and comparably folded. *deg*, degrees.

TABLE 3

Kinetic parameters of GTP hydrolysis reactions for full-length and truncated forms of the alphaviral nsP2

Enzyme (Ref.)	K_m	K_{cat}	K_{cat}/K_m	K_{cat}/K_m
	μM	/s	/s·M	% of nsP2
CHIKV nsP2 (this study)	13.32 ± 1.01	57.69	4.33×10^6	100
CHIKV His-nsP2 (this study)	18.36 ± 1.78	10.73	0.58×10^6	13
CHIKV N470 (this study)	11.77 ± 2.39	10.78	0.91×10^6	21
CHIKV aa residues 167–630 (11)	0.03[a]	0.50		
SFV aa residues 1–470 (9)	90	~4	0.04×10^6	~1

[a] The K_m value was 29.1 nM, so only the basal K_{cat} value was compared with other studies.

To determine the kinetic parameters of the purified recombinant enzymes, the concentration of Mg^{2+} was optimized with respect to the ATP substrate. ATP hydrolysis by N470 was active over a wide range of Mg^{2+} concentrations. However, the highest activity was observed at a Mg^{2+}:substrate concentration ratio of 6:1 (Fig. 3*B*), which was used for subsequent experiments. Although the observed differences in ATP and GTP hydrolysis were minor (Fig. 3*A*), GTP was used in the experiments measuring the kinetic parameters of NTPases because this substrate has been used in previous studies addressing NTPases of alphaviruses (Table 3). The K_m and K_{cat} values were determined by measuring the GTP hydrolysis rate at varying substrate concentrations (1–200 μM; Fig. 3*C*). The initial velocities were linear over a period of several minutes, thus enabling measurement of the reaction rate. This analysis revealed that the rate of GTP hydrolysis by N470 was higher than has been reported previously for the N-terminally tagged 470-aa-long fragment of SFV nsP2 (Table 3). Furthermore, CHIKV nsP2 was found to be an even more efficient NTPase than N470 or His-nsP2, whose activities were only 21 and 13% of the activity of nsP2, respectively (Table 3). Unlike the data from previous reports (9, 11), the high basal activity of nsP2 detected in this study was within the expected range for the SF1 viral helicase (31). In our experiments, nsP2-delNTD and nsP2-delMTL were not capable of performing NTP hydrolysis (data not shown). However, because these proteins also showed signs of aggregation (as evidenced by elution profiles in size exclusion chromatography and CD spectroscopy data analysis (data not shown)), it is not possible to reconcile whether NTD and MTL accessory domains located outside of the RecA-like core may contribute to the coordination of NTP hydrolysis by nsP2. On the other hand, it was found that deletion or addition of few aa residues as in the case of nsP2-delN2 or nsP2-insN2 resulted in active enzymes, although their ability to perform GTP hydrolysis was clearly reduced (Fig. 3*D*).

The activities of the many viral NTPases can be stimulated by the presence of RNA or DNA, although the extent of the stimulatory effect may differ considerably. To determine the potential stimulatory effects of various RNA and DNA homo-oligomers, the NTPase activities of N470, His-nsP2, and nsP2 were analyzed in the presence of oligonucleotides 8–11 (Table 1). This analysis revealed that the effect of all of these oligonucleotides on the NTPase activity of N470 was rather minor, and the maximum stimulation was observed in the presence of poly(U) oligonucleotides (Fig. 3*E*). The effects of the oligonucleotides on the NTPase activity of His-nsP2 and nsP2 were more prominent. For both proteins, the maximum stimulatory effect was observed in the presence of poly(dC) and poly(dG) oligonucleotides (up to 2.5-fold). In contrast, the presence of poly(G) oligonucleotide appeared to reduce the activity of these enzymes (Fig. 3*E*). Similar levels of stimulation were also observed for the nsP2-delN2 and nsP2-insN2 mutants (data not shown). Notably, comparable moderate degrees of stimulation have been reported previously for a recombinant protein corresponding to a fragment of ns polyprotein from Rubella virus (53), which also belongs to the Togaviridae family of viruses.

Taken together, it can be concluded that both the authentic N-terminal region and the C-terminal part of nsP2 contribute to the specific activity of its NTPase domain. This may result

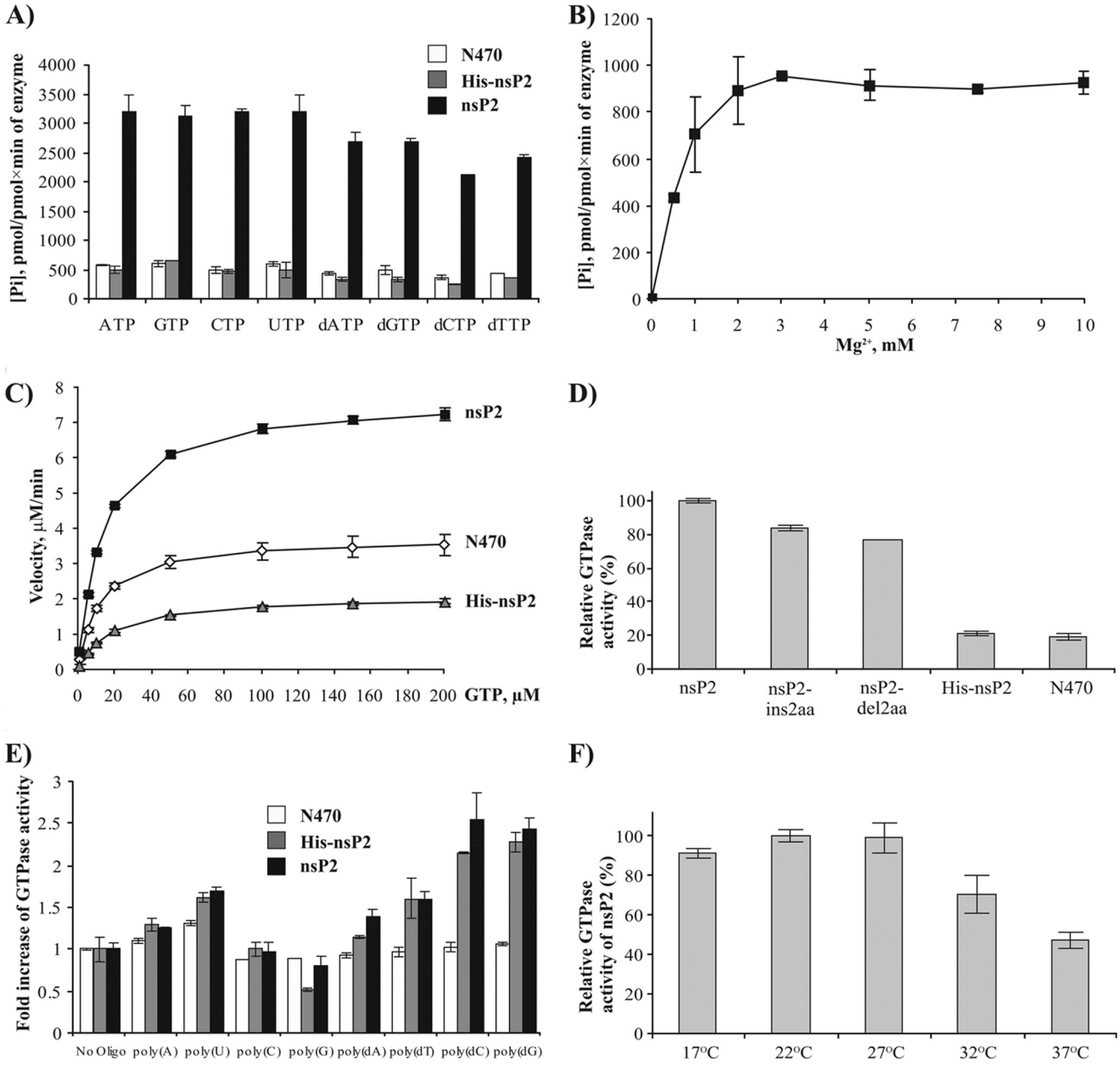

FIGURE 3. **Analysis of the NTPase activity of the obtained recombinant enzymes.** *A*, specific NTPase activities of N470, His-nsP2, and nsP2 in the presence of 100 μM concentrations of different NTP or dNTP substrates. *B*, optimization of Mg^{2+} concentration for the NTPase activity of N470. The reactions were conducted using 500 μM ATP as a substrate and different concentrations of Mg^{2+}. *C*, determination of the kinetic parameters of NTPase reactions. A plot of initial velocity (*vertical axes*) *versus* GTP concentration (*horizontal axes*) in GTPase reactions for N470, His-nsP2, and nsP2 is shown. The determined kinetic parameters are summarized in Table 3. *D*, relative GTPase activities of the N470 and different nsP2 variants compared with the activity of WT nsP2. *E*, effects of the different RNA or DNA homo-oligomers on the GTPase activity of N470, His-nsP2, and nsP2. The final concentration of each oligonucleotide in the reaction mixture was 1.75 μM. *F*, temperature dependence of the GTPase activity of nsP2. The data presented in each panel represent the average of at least three independent experiments; *error bars* represent S.D.

from either the stabilization of a favorable active conformation of the enzyme or the provision of additional structural elements. The presence of the C-terminal part of nsP2 also clearly increased the stimulatory (or in the case of poly(G), inhibitory) effect of the oligonucleotides on the NTPase activity potentially by providing a binding platform for interactions with these nucleic acids (Fig. 3*E*). Therefore, the presence of the C-terminal domains in this protein with NTPase/helicase activity is not accidental. Furthermore, the authentic N terminus of nsP2, which has been shown to play a crucial role in the regulation of the protease activity of nsP2 (30), is similarly important for its NTPase activity.

The Full-length Forms of NsP2, but Not N470, Possess 5′–3′ RNA Helicase Activity—To initiate the unwinding of ds substrates, a helicase must bind to the sugar-phosphate backbone in a specific orientation. This binding orientation determines the classification of helicases based on their polarity (54). To reveal substrate specificity and polarity of the CHIKV nsP2 helicase, a set of DNA and RNA oligonucleotides (Table 1) was used to generate substrates with identical 16-base pair ds

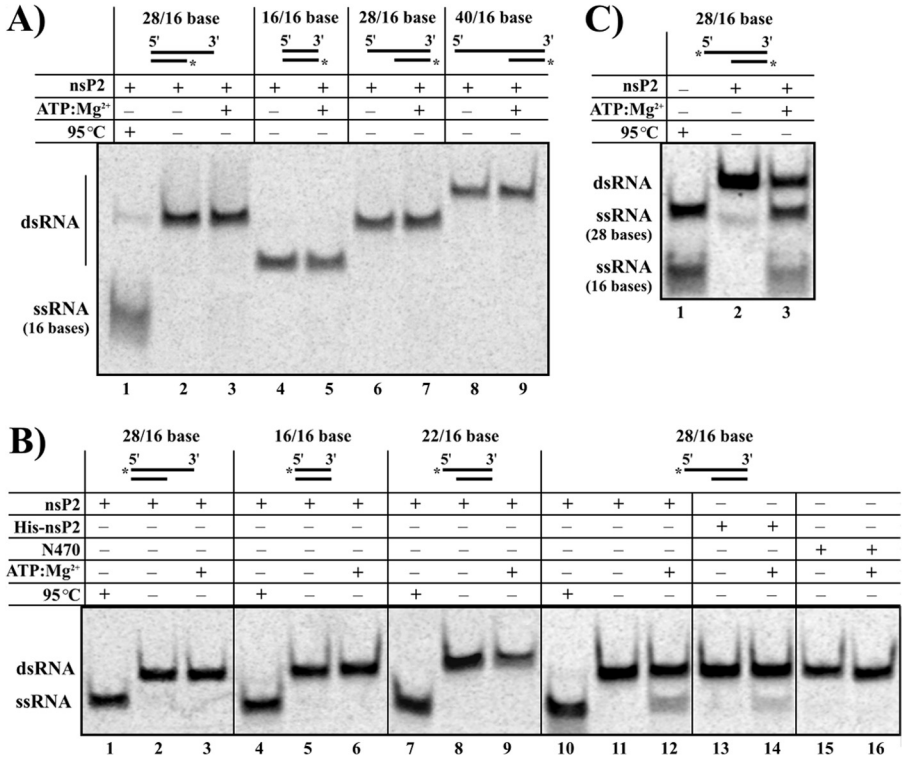

FIGURE 4. **NsP2 exhibits 5′–3′ directional RNA helicase activity.** *A*, NsP2 lacks DNA helicase activity. The assay was conducted using different dsDNA substrates at 50 pM concentration and 12.5 nM nsP2 in the presence or absence of 3.5 mM ATP-Mg^{2+}. *Lane 1*, the sample denatured by heating at 95 °C was used as the marker for 16-base ssDNA molecules. *B*, nsP2 is a 5′ overhang-dependent RNA helicase. The assay was performed using different types of dsRNA substrates at 50 pM concentration and 12.5 nM nsP2, His-nsP2, or N470 in the presence or absence of 3.5 mM ATP-Mg^{2+}. *Lanes 1*, *4*, *7*, and *10*, the sample was denatured by heating at 95 °C and used as a marker for ssRNA molecules. *C*, nsP2 releases both ssRNAs from the dsRNA substrate. The experimental conditions were identical to those shown in *B* except that both strands of the substrate with the 12-base 5′ overhang were labeled. The labeling of the 16-base ssRNA reproducibly resulted in an artifact band (visible on *lane 2*) at a position that corresponded almost exactly to that of the labeled 28-base ssRNA. The helicase activity of nsP2, however, is clearly evident from the increase in the signal intensity at the position corresponding to 28-base ssRNA as well as from the displacement of 16-base ssRNA (*lane 3*). * denotes a 5′ ^{33}P label on the indicated oligonucleotides. Each panel represents data from one of three highly reproducible experiments.

regions but different 5′ and/or 3′ overhangs. In a standard helicase assay, the molar ratio of enzyme to substrate was maintained at 250:1 to allow the excess of the enzyme to act as a ssRNA- or ssDNA-binding protein to prevent the displaced strands from reannealing to their complements (55, 56).

NsP2 was unable to unwind any of the tested dsDNA substrates (Fig. 4*A*) in contrast to the NS3 helicase of hepatitis C virus (this protein, analogous to previously described (57), was purified in house), which efficiently unwound the dsDNA substrate with a 12-base 3′ overhang (data not shown). NsP2 was also unable to unwind dsRNA substrates with a 12-base 3′ overhang, blunt ends, or a 6-base 5′ overhang. However, this protein was capable of unwinding the dsRNA substrate with the 12-base 5′ overhang (Fig. 4, *B* and *C*). Thus, CHIKV nsP2 displays RNA helicase activity with a 5′–3′ polarity. Furthermore, based on the length of the 5′ overhangs examined here, an occlusion size of nsP2 between 7 and 12 bases can be proposed. Comparison of the RNA helicase activity of nsP2 with that of His-nsP2 revealed that our results were in accord with the previous findings for the tagged SFV nsP2 (14) as CHIKV His-nsP2 was also capable of unwinding dsRNA substrates with the 12-base 5′ overhang (Fig. 4*B*). Remarkably, although N470 possessed greater NTPase activity than His-nsP2 (Table 3), it evidently lacked RNA helicase activity (Fig. 4*B*). This finding is also consistent with the lack of helicase activity observed for truncated CHIKV nsP2 (11). Therefore, it can be concluded that the presence of the C-terminal part of nsP2 is an absolute requirement for the RNA helicase activity of this protein. Thus, both the RNA helicase and to a lesser extent NTPase activities of nsP2 depend not only on the narrowly defined "NTPase region" but also on the remote elements of this protein as well.

The N-terminal His_6 Tag Affects dsRNA Unwinding by CHIKV NsP2—The presence of a small affinity tag had a profound effect on the NTPase activity of nsP2 (Fig. 3, *A* and *C*, and Table 3). To reveal whether this is also the case for the RNA helicase activity of nsP2, the kinetics of RNA helicase reactions were analyzed for different types of dsRNA substrates. Both nsP2 and His-nsP2 were capable of unwinding the dsRNA substrates with rather similar kinetics (Fig. 5*A*). During the first 30 min, the reactions generally approached equilibrium (Fig. 5*A*), similarly to the previous observations for other helicases (58). The observed plateau levels depended on the types of enzyme and substrate involved, and increasing the enzyme-to-substrate ratio from 250:1 to 1000:1 failed to shift the equilibrium considerably (Fig. 5*B*). Comparison of the abilities of nsP2 and His-nsP2 to unwind different RNA substrates consistently revealed that His-nsP2 was capable of unwinding a smaller amount of dsRNA than nsP2 (Table 4). However, the effect of the N-terminal tag on RNA helicase activity was relatively mild compared with its effect on NTPase activity (Fig. 3*A* and Table 3). In

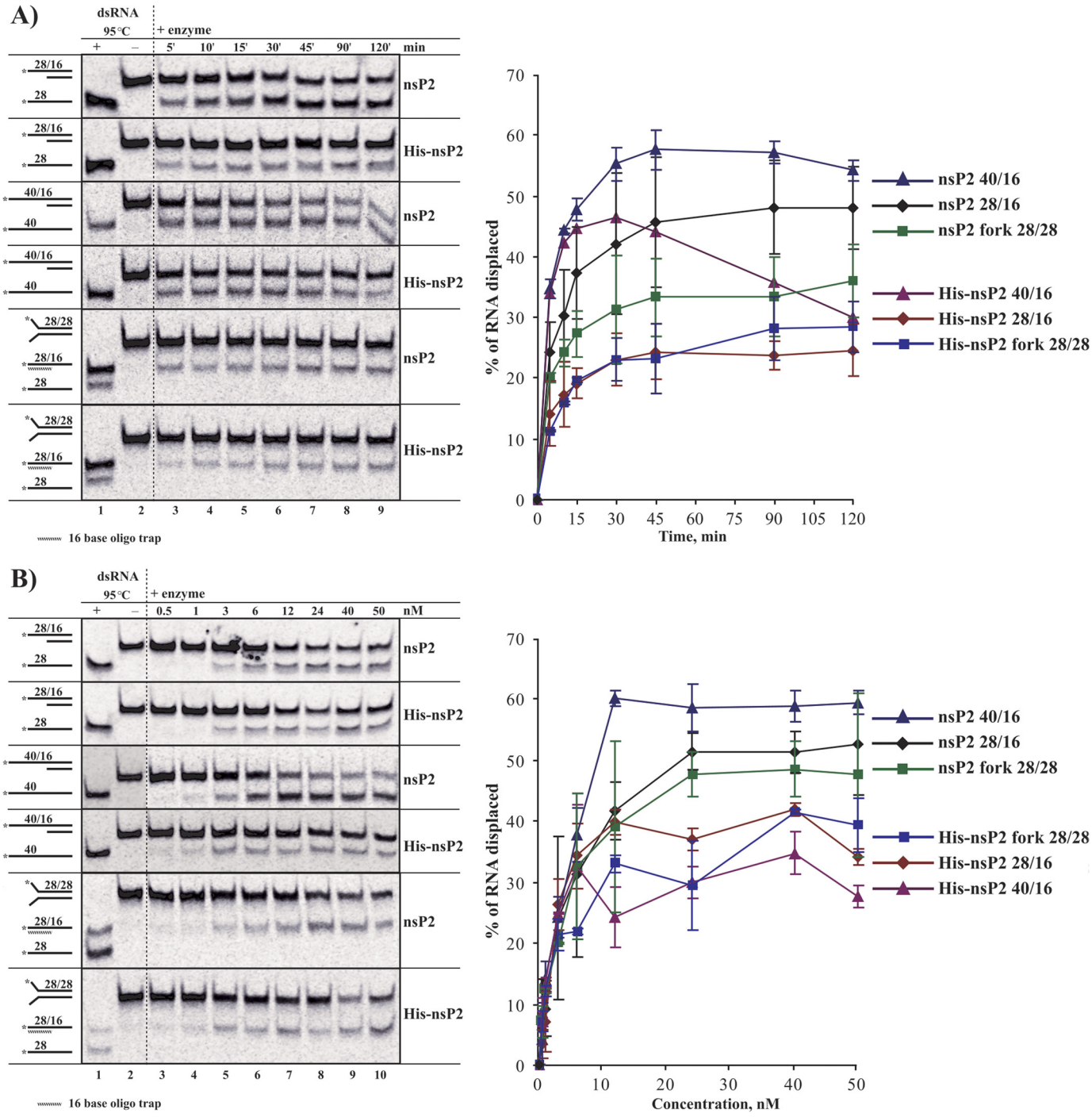

FIGURE 5. **Time and enzyme concentration dependence of the dsRNA unwinding activities of nsP2 and His-nsP2 for different dsRNA substrates.** The assay was conducted using different types of dsRNA substrates at 50 pM and 12.5 nM nsP2 or His-nsP2 in the absence (*lane 2*) or presence (*lanes 3–9*) of 3.5 mM ATP-Mg^{2+}. The dsRNA heated at 95 °C was used as marker for ssRNA (*lane 1*). * denotes a 5′ ^{33}P label on the indicated oligonucleotides. The *left panels* of *A* and *B* show representative gel pictures, whereas the *right panels* show the quantitative measurement of ssRNA displacement. The *error bars* in the *right panels* represent the S.D. of the data from three independent experiments. *A*, the reaction was performed in a final volume of 60 μl, and 5-μl aliquots were collected at the indicated time points and analyzed by 15% PAGE. *B*, the experimental conditions were the same as for *A* except that the final reaction volume was 5 μl, the concentrations of enzymes varied from 0.5 to 50 nM, and the reaction time was 120 min. Note that for the fork substrate the primary reaction product is the dsRNA containing the labeled 28-base strand and the unlabeled 16-base strand that was used as a trap RNA. This dsRNA exhibits a 3′ overhang and cannot be unwound by nsP2.

line with these findings, the nsP2-insN2 and nsP2-delN2 mutants were also found to have RNA helicase activities essentially indistinguishable from that of nsP2 (data not shown).

NsP2 Is a 5′ Overhang-dependent Non-processive Helicase—In contrast to the 12-base 5′ ss region, the 24-base 5′ ss region of the dsRNA substrate may potentially accommodate multiple copies of nsP2 molecules. It was hypothesized that if nsP2 possesses low processivity and tends to fall off from its substrate then extension of the ss region may result in more efficient substrate unwinding because trailing nsP2 molecules would

TABLE 4

Kinetic parameters calculated from the RNA unwinding (Uw) and rewinding (Rw) experiments

$P5'_{Uw}$ and $P15'_{Rw}$, percentage of ssRNA and dsRNA formed at 5 and 15 min, respectively; A_{Uw} and A_{Rw}, final reaction amplitude.

	Unwinding				Rewinding[a]			
	NsP2		His-nsP2		NsP2		His-nsP2	
Types of substrate	$P5'_{Uw}$	A_{Uw}	$P5'_{Uw}$	A_{Uw}	P15′Rw	A_{Rw}	$P15'_{Rw}$	A_{Rw}
	% of ssRNA formed				*% of dsRNA formed*			
12-Base 5′ overhang	24.3 ± 5.0	48.0 ± 6.7	14.2 ± 5.4	24.6 ± 4.3	3.5 ± 1.8	9.8 ± 0.4	23.9 ± 0.4	45.4 ± 1.0
24-Base 5′ overhang	34.7 ± 1.7	54.3 ± 1.7	33.9 ± 0.3	29.9 ± 2.3[b]	11.4 ± 1.9	16.7 ± 4.3	30.4 ± 2.5	39.5 ± 1.5
12-Base 3′ and 5′ overhangs (fork)	20.1 ± 0.8	36.1 ± 6.1	11.3 ± 0.1	28.5 ± 4.3	30.0 ± 0.2	47.1 ± 0.7	47.4 ± 3.6	64.3 ± 0.1

[a] The activities represent the difference between the amount of dsRNA formed in the presence and absence of the enzyme.
[b] In this reaction, the maximal reaction amplitude was 46.5 ± 1.9% (Fig. 5*A*).

replace molecules dissociated from the substrate, thereby reducing the probability of discontinuous unwinding (59). In support of this hypothesis, a larger fraction of the substrate with a 24-base 5′ overhang was unwound compared with the substrate with the 12-base 5′ overhang (Fig. 5, *A* and *B*, and Table 4). These experiments also revealed that when His-nsP2 was used to unwind the substrate with the 24-base 5′ overhang the unwinding reached its maximal amplitude (~46%) after ~30 min, and then the decrease in the amount of ssRNA product was observed (Fig. 5*A* and Table 4).

NsP2 Possesses Intrinsic RNA Annealing Activity That Is Enhanced by the Presence of the His_6 Tag—The observation that the formation of the ssRNA product occurred rapidly only during the first 10–15 min of the reaction (Fig. 5*A*) led to the hypothesis that nsP2 may exhibit intrinsic RNA annealing activity, preventing the unwinding reaction from proceeding beyond the observed plateau level. RNA annealing activity is reportedly an ATP-independent process (60). Therefore, the recombinant proteins were assayed in reactions performed in the absence of ATP at 22 °C under a low salt concentration (0.5 mM Mg^{2+} and 1 mM NaCl) using different heat-denatured dsRNAs as substrates. In the absence of any enzyme, slow and inefficient spontaneous formation of dsRNA was observed (Fig. 6). The presence of N470 in the reaction mixture did not have any effect on this process, indicating that this recombinant protein lacks RNA annealing activity. In contrast, clear RNA annealing activity was observed for both nsP2 and His-nsP2 (Fig. 6 and Table 4). NsP2 was relatively inefficient in carrying out the reaction with substrates leading to the formation of dsRNA with a 12-base 5′ overhang (Fig. 6*A*). Furthermore, nsP2 performed only slightly better in the reaction that led to the formation of dsRNA with a 24-base 5′ overhang (Fig. 6*B*). Consistent with previous reports regarding enzymes with RNA annealing activity (60, 61), the highest nsP2 annealing activity was observed for substrates leading to formation of dsRNA with fork structure (Fig. 6*C*). Simultaneously, His-nsP2 always demonstrated more robust and less substrate-specific RNA annealing activity, which might be caused by the presence of extra positive charges at its N terminus. These data also indicated that the enhanced RNA annealing activity of His-nsP2 may be one of the reasons for the reduced levels of the dsRNA unwinding observed for this recombinant protein (Fig. 5).

The Presence of a His_6 Tag Increased the Salt Tolerance of NsP2 RNA Helicase Activity—One of the key differences between the NTPase and RNA helicase reactions is the modulation of NTP and RNA binding because in the latter case the enzyme must bind RNA along with NTP. Because of its extra positive charge, the His_6 tag may facilitate the binding of negatively charged dsRNA (62). To verify this hypothesis experimentally, the ability of nsP2 and His-nsP2 to unwind the dsRNA substrate with a 12-base 5′ overhang was assayed in the presence of 8–163 mM NaCl (taking into consideration the NaCl concentration present in the protein storage buffer). NsP2 demonstrated robust helicase activity at a salt concentration ≤16 mM. At higher concentrations, its enzymatic activity declined rapidly, becoming undetectable at concentrations ≥65 mM NaCl (Fig. 7*A*). In contrast, His-nsP2 was remarkably more resistant to increased concentrations of NaCl, and almost no decrease in helicase activity was observed within NaCl concentrations ranging from 65 to 163 mM (Fig. 7*A*). Thus, the positively charged His_6 tag evidently results in tolerance of the interactions between the enzyme and RNA up to a high concentration of salt. In contrast, when the helicase activities were analyzed at different pH values, no notable difference was detected between the behavior of nsP2 and His-nsP2, and both enzymes were active over a wide range of pH values (6.0–9.5), showing a slight peak at pH 7.2 (Fig. 7*B*).

Helicase Activity of NsP2 Does Not Depend on the Type of NTP or dNTPs but Is Dependent on the Presence of Mg^{2+} Ions—As the different forms of nsP2 of CHIKV were able to use all NTPs and dNTPs as substrates in the NTPase reaction (Fig. 3*A*), it was expected that helicase activity of nsP2 can be fueled from the hydrolysis of any of these nucleotides. To analyze this directly, the RNA helicase activities of nsP2 and His-nsP2 were assayed in the presence of different canonical NTPs and dNTPs. As expected, both nsP2 and His-nsP2 showed comparable RNA helicase activity with all these substrates; if anything, the UTP, dCTP, and dGTP were slightly less favored (Fig. 7*C*).

Similarly, the dependence of nsP2 RNA helicase activity on different types of metal ions was analyzed. Mg^{2+} was the clearly preferred divalent metal cation, and some preference for magnesium acetate over chloride was also observed (Fig. 7*D*). All of the other tested divalent cations (Mn^{2+}, Zn^{2+}, and Ca^{2+}) as well as Fe^{3+} and Cs^{+} resulted in strongly diminished and nearly equivalent RNA helicase activities of both nsP2 and His-nsP2.

NTPase and Helicase Activities Are Influenced by Temperature Conditions—Alphaviruses normally shuttle between insect vector and mammalian host, which have significantly different body temperatures. Therefore, although the helicase reactions in this study were performed at physiologically relevant temperature of 37 °C (after preincubation at 22 °C to facilitate protein-RNA complex formation), it was essential to estimate the

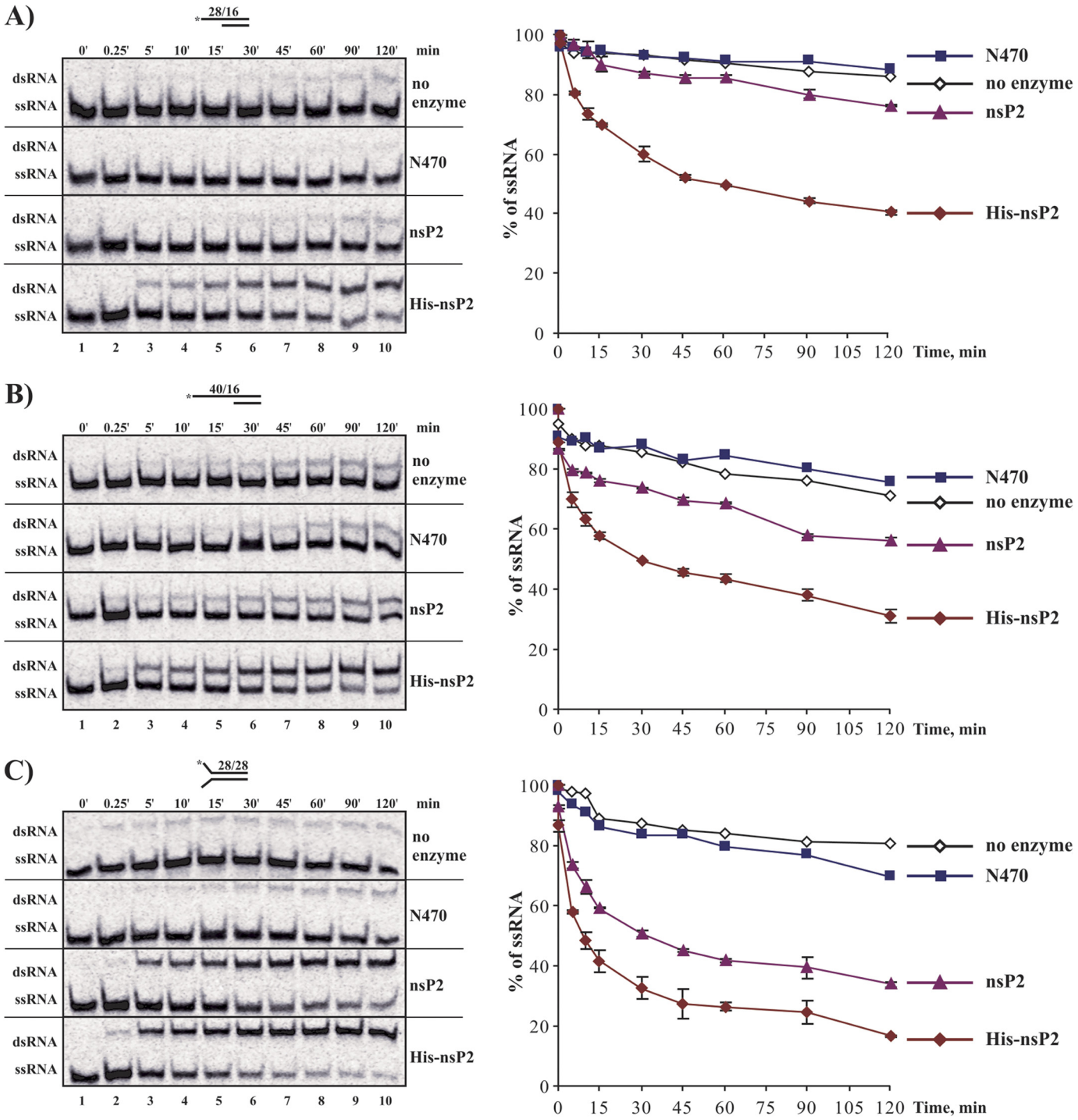

FIGURE 6. **NsP2 exhibits RNA strand annealing activity.** ssRNAs (50 pM) obtained through heat denaturation of the indicated dsRNAs were used as the substrates for testing the RNA annealing activity of N470, nsP2, or His-nsP2 at a 12.5 nM concentration. The reactions were carried out at 22 °C in the presence of 0.5 mM Mg^{2+} and 1 mM NaCl in a final volume of 60 μl. Control reactions were performed under the same conditions except that no enzyme was added. At the indicated time points, 5-μl aliquots were collected and analyzed by 15% PAGE. The dsRNA heated at 95 °C (without incubation at 22 °C) was used as marker for ssRNA (*lane 1*). The *left side* of each panel provides representative gel images for the corresponding experiments. The *right side* of each panel provides the quantitative measurements obtained for the remaining labeled ssRNAs over the period of the experiment. The *error bars* represent the S.D. of the data from three independent experiments. *A*, annealing of the oligonucleotides forming dsRNA with a 12-base 5′ overhang. *B*, annealing of the oligonucleotides forming dsRNA with a 24-base 5′ overhang. *C*, annealing of the oligonucleotides forming dsRNA with a 12-base fork structure. * denotes a 5′ ^{33}P label on the indicated oligonucleotides.

temperature dependence of the enzymatic reactions. Additionally, the standardization of the assay for inhibitors screening would benefit from the knowledge about the maximal expected activity and possible data variation due to temperature fluctuations. To this end, we observed a typical bell-shaped temperature dependence of the GTPase activity of nsP2. The enzyme performed almost 2 times better in the temperature interval of 22–27 °C than at 37 °C (Fig. 3*F*). The helicase activity of nsP2

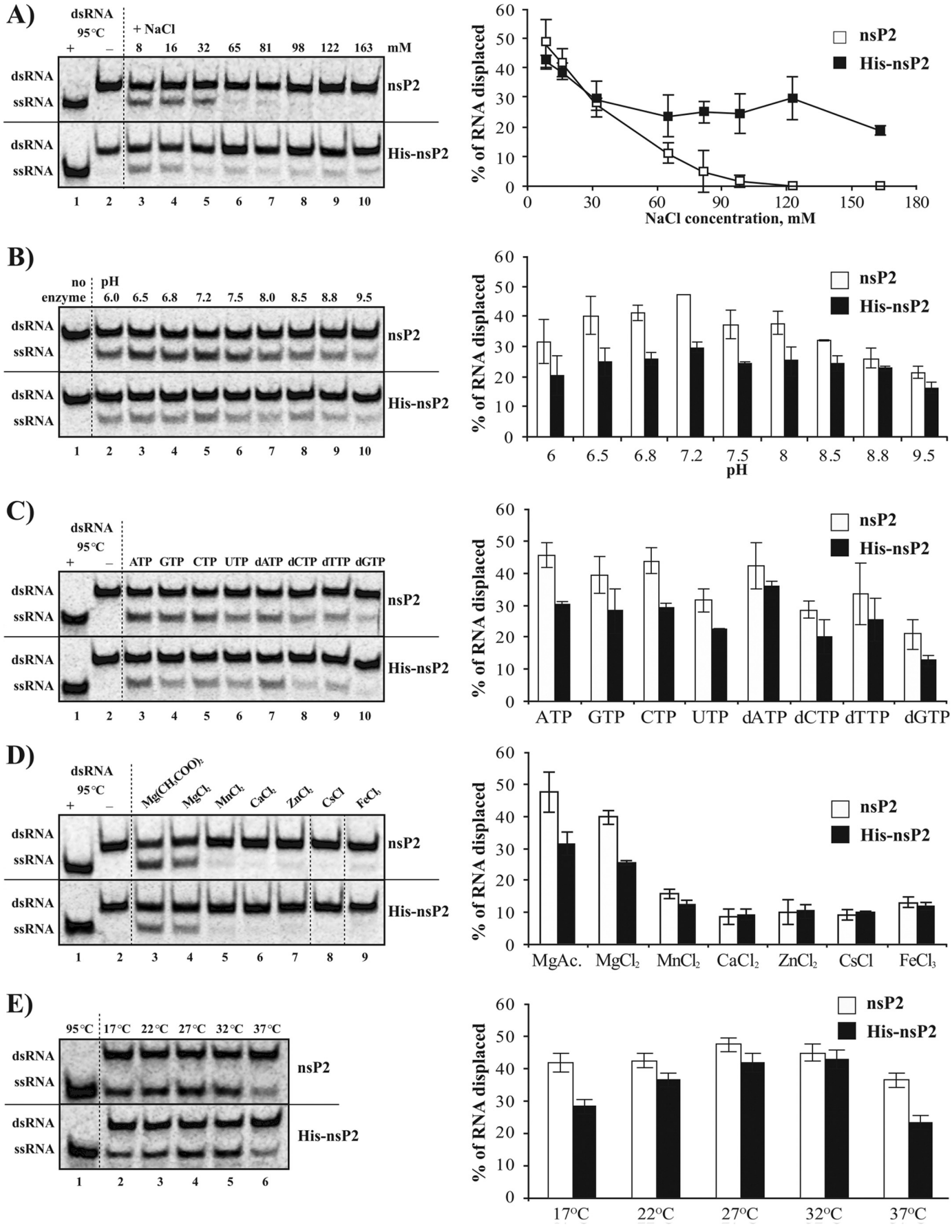
A)
dsRNA 95°C
+ NaCl
+ – 8 16 32 65 81 98 122 163 mM
dsRNA
ssRNA
nsP2
His-nsP2
1 2 3 4 5 6 7 8 9 10
% of RNA displaced
NaCl concentration, mM
B)
no enzyme
pH 6.0 6.5 6.8 7.2 7.5 8.0 8.5 8.8 9.5
pH
C)
ATP GTP CTP UTP dATP dCTP dTTP dGTP
D)
MgAc. MgCl2 MnCl2 CaCl2 ZnCl2 CsCl FeCl3
E)
95°C 17°C 22°C 27°C 32°C 37°C
17°C 22°C 27°C 32°C 37°C

was also affected by temperature variation, showing the maximum around 27 °C, whereas the temperature dependence profile for helicase activity of His-nsP2 was somewhat different (Fig. 7*E*), again suggesting a difference in the properties of these two enzymes. Thus, it can be concluded that future inhibition studies should be most optimally performed at room temperature (22–25 °C) at which the enzymatic activities of nsP2 remain stably maximal.

DISCUSSION

Alphaviral nsP2 is a multifunctional protein, and it has been classified as an SF1 helicase based on its sequence (24, 63). Here, we demonstrated that recombinant full-length CHIKV nsP2 with a native N terminus showed high basal NTPase activity, 5′–3′ directionally biased RNA helicase activity, and RNA rewinding activity. His-nsP2, a variant of nsP2 with an N-terminal His_6 tag, possessed reduced RNA unwinding activity and enhanced rewinding activity as well as strongly reduced NTPase activity. N470, a protein lacking the C-terminal region of nsP2, displayed similarly reduced NTPase activity but no detectable RNA-modulating activity. Our findings provide an explanation for previous observations, such as the moderate NTPase and RNA triphosphatase activities detected for a recombinant protein consisting of the 470 N-terminal aa residues of SFV nsP2 with an N-terminal affinity tag (9, 10) and the failure to observe RNA helicase activity for the truncated form of nsP2 (11). The three-dimensional molecular modeling (Fig. 1*B*) and sequence analysis (Fig. 1*C*) confirmed the presence of classical NTPase/helicase motifs in the predicted RecA-like domains of nsP2. As expected, point mutations at critical aa residues within these motifs completely abolished the NTPase activity of the enzyme. However, it is less obvious how regions located at some distance from the NTPase catalytic center contribute to the RNA-modulating and NTPase activities of the protein.

Bioinformatics predictions of the three-dimensional structure of the nsP2 N-terminal region failed to reveal a putative domain that may bind RNA in a manner similar to the 1C domain in Upf1 (45); and accordingly, the stimulatory effect of nucleic acids on the NTPase activity of N470 was minimal (Fig. 3*E*). In contrast, NTPase activities of both nsP2 and His-nsP2 were more responsive to the presence of oligonucleotides. Two additional domains are present in these proteins compared with N470. The penultimate papain-like protease domain of nsP2 exhibits an isoelectric point (pI) of ~8.4, whereas the MTL domain of nsP2 has a calculated pI of ~10.13, thus becoming a likely candidate for a nucleic acid-binding domain. Furthermore, electrostatic interactions may exist between the MTL domain and the NTD (pI ~ 5.4). Consistent with this hypothesis, the recombinant protein corresponding to aa residues 167–630 of CHIKV nsP2, and thus containing the papain-like protease domain but lacking the MTL domain, was previously reported to completely lack RNA helicase activity (11). Thus, our results suggest that the MTL domain is responsible for RNA-binding activity.

Coexistence of the protease and helicase modules in the same unit is a common theme in the organization of the viral proteins. To this end, certain parallels can be drawn from the studies of the NS3 proteins from viruses belonging to the Flaviviridae family. These proteins also contain both helicase and protease domains, and several studies have suggested the existence of functional interplay between these domains (27–29). For example, in the case of NS3 of hepatitis C virus, the protease domain was found to contribute to NTPase activity by increasing the RNA binding affinity of the protein (27, 62). Similarly, the helicase activity of the full-length NS3 of dengue virus 2 was enhanced in comparison with that of the helicase domain only (64), whereas any mutation in the protease-helicase interdomain region was found to drastically affect helicase activity, therefore providing evidence of cross-talk between the protease and helicase domains (29, 65). Notably, a previous study using alanine scanning of the positively charged residues in the MTL domain of Sindbis virus (alphavirus) nsP2 revealed very different effects of these substitutions on the infectivity of viral RNA, virus growth characteristics, and polyprotein processing (66). Importantly, several of these mutants showed severe defects with lethal or temperature-sensitive phenotypes, indicating perturbations in most important viral functions. It can be assumed that the unexplained behavior of several of these mutants is due to, at least in part, disturbed helicase/NTPase functionality, which is critically linked to the properties of the MTL domain. Therefore, it is appealing to revisit conclusions from this previous study in light of our new findings.

In line with previous observations (20, 30), our experiments also highlighted the importance of the native N terminus of the nsP2 for NTPase and helicase activities. In the course of viral replication, the N terminus of nsP2 is liberated from the ns polyprotein after *in cis* cleavage of the nsP1/nsP2 junction by the protease activity of nsP2. This intramolecular process intrinsically relies on the bringing the N-terminal-most part of nsP2 toward the protease and MTL domains, both of which contribute to substrate recognition for proteolysis (43, 67, 68). Specific contacts apparently lead to hiding of the N terminus of

FIGURE 7. **Effects of different NaCl concentrations, pH, nucleotides, metal ions, and temperature conditions on the RNA helicase activity of nsP2 and His-nsP2.** *A*, the effect of the NaCl concentration on helicase activity was analyzed using 80 pM dsRNA substrates and 20 nM nsP2 and His-nsP2. The reaction mixtures contained 3 mM ATP-Mg^{2+} and the indicated concentrations of NaCl, also taking into account the amount of NaCl present in the protein storage buffer. *B*, the effect of pH on the helicase activity was analyzed in reactions containing 50 pM dsRNA substrate, 12.5 nM enzyme, and 3.5 mM ATP-Mg^{2+} at the indicated pH levels. *C*, the effect of NTPs and dNTPs on the helicase activity of nsP2 was analyzed in reactions containing 50 pM dsRNA substrate, 12.5 nM enzyme, 3.5 mM Mg^{2+}, and a 3.5 mM concentration of each NTP or dNTP. *D*, the effect of different metal ions on the helicase activity was analyzed in reactions containing 50 pM dsRNA substrate, 12.5 nM enzyme, the indicated metal acetate or chloride at 3.5 mM, and 3.5 mM ATP. *E*, the effects of the temperature conditions on the helicase activity of nsP2 were analyzed in reactions containing 50 pM dsRNA substrate, 12.5 nM enzyme, and 3.5 mM ATP-Mg^{2+} at the indicated temperature. In all of the experiments, the dsRNA with the 12-base 5′ overhang was used as a substrate. The *left side* of each panel provides representative gel images obtained for nsP2 and His-nsP2. The dsRNA heated at 95 °C was used as a marker for ssRNA (*lane 1*). The control samples to which no ATP-Mg^{2+} was added were used as the markers for the dsRNA in *A*, *C*, and *D* (*lane 2*). The sample from the control reaction that proceeded without enzyme was used in *B* (*lane 1*). The *right side* of each panel shows the quantitative measurements for the corresponding experiments for nsP2 and His-nsP2. The *error bars* in the *right panels* represent the S.D. of the data from three independent experiments.

nsP2 in the interdomain environment, thus explaining our findings that the N-terminal region of His-nsP2 was shielded from external access by TEV protease, whereas in the similarly His_6-tagged nsP2-delMTL and N470 constructs, the TEV cleavage site was easily accessible. Based on our results, it can be envisioned that the N-terminal segment of nsP2 contributes to the stabilization of such conformation of nsP2 that allows for its maximal enzymatic activity, whereas deletion or addition of just a few aa residues, as in the case of nsP2-insN2 and nsP2-delN2, already has an effect on enzymatic properties (Fig. 3*D*). CD spectroscopy analysis revealed that all these proteins were sufficiently well folded. Nevertheless, this method did not reveal any significant structural differences between protein variants (Fig. 2*B*). This implies that fine conformational adjustments affecting the cross-talk between contributing elements could be responsible for the observed changes in enzymatic properties. In combination with the discovery that the artificial N-terminal His_6 tag had a profound effect on the NTPase activity of nsP2, it can therefore be strongly suggested that specific attention should be paid to ensure the most native conformation of the alphaviral nsP2 for proper enzymatic profiling.

During the course of viral infection, the cleavage of the nsP1/nsP2 site is believed to cause a switch in the template preference of the viral replication complex, and the RNA synthesizing activity then becomes directed toward the production of positive strands of RNA (4, 69). Curiously, in the case of the poliovirus 2C ATPase, it was clearly demonstrated that its enzymatic properties are modulated by the polyprotein context: maximal activity of 2C is achieved upon proteolytic removal of the adjacent domains (70). In this context, it remains to be demonstrated to what extent the NTPase and helicase abilities of the P123 polyprotein may differ from those of mature nsP2 and whether nsP1/nsP2 cleavage may activate one of these previously possibly inhibited functions. Also, inside the cell, mature nsP2 is present in the cytoplasm, in the nucleus (71), and within the virus replication-induced spherules, which are first assembled at the plasma membrane and then become fused with endolysosomes (72). Given that the optimal conditions for the various enzymatic activities of nsP2 are not identical (9) and *e.g.* nsP2 helicase demonstrates sensitivity to salt concentration (Fig. 7*A*), it is plausible to suggest that the ability of nsP2 to perform its various functions inside the host cell is also likely regulated by the different subcellular environmental conditions.

The significance of the RNA helicases in the life cycle of positive-strand RNA viruses, including alphaviruses, is poorly understood. Different forms of long dsRNAs, sometimes collectively referred to as replicative intermediates (RIs), are produced in alphavirus-infected cells (2). However, it remains unknown whether helicases act as unwinding and rewinding machines on these dsRNAs (73) or only act to melt short secondary structure elements that may be formed during various stages of viral RNA synthesis. Additionally, RNA-dependent ATPases or RNA helicases may perform single strand translocation (74), protein displacement, ribonucleoprotein complex remodeling (75, 76), or RNA chaperone activity, assisting in RNA conformational rearrangements (60). This uncertainty is, at least in part, caused by the fact that NTPase, helicase, and RNA triphosphatase activities needed for RNA capping are all attributed to (or are fueled by) the same reaction center, which complicates dissection of their functional significance for viral infection through introduction of mutations in Walker motifs. To this end, in a previous study, the SFV genome that was engineered to contain a mutation in the conserved Walker A motif (K192N) demonstrated severely reduced infectivity but was able to undergo reversion and produce infectious progeny (77). Because reversions in the viral genome are only possible if the virus is capable of RNA copying at all, it can be concluded that the activities associated with the NTP-binding site of nsP2 are possibly dispensable for at least some early stages of viral RNA replication during which genome repair becomes possible. In principle, the reported ability of alphaviral nsP4 to copy minus and plus strands of RNA in the absence of other viral proteins creates the necessary prerequisites for fixing the mutated genome (78). Still, because of the above mentioned reasons, it remains to be revealed which of the enzymatic activities of SFV nsP2 affected by Walker motif mutation was most critical and required a repair to restore virus infectivity.

The data and conclusions presented above provide possibilities for speculations regarding the role of RNA helicase activity in alphavirus infection. It appears highly probable that nsP4, which synthesizes RNA in the 5′–3′ direction, and nsP2, which unwinds RNA in the same direction, may act in a coordinated manner. Furthermore, the replication of the alphavirus genome occurs through the synthesis of the negative RNA strand with extra, untemplated G residue at its 3′ end (79). It was recently also shown that the initiation of negative RNA strand synthesis occurs at the last C residue before the poly(A) tail of the virus genome (80). Thus, the dsRNA RIs produced in alphavirus-infected cells exhibit 3′ overhangs at both ends, which makes it impossible for nsP2 to contribute to initiation of RNA replication by unwinding these duplexes. Detailed Venezuelan equine encephalitis virus replication studies have revealed, however, that the 3′ end of the negative RNA strand and the 5′ end of the positive RNA strand most likely form a structure with both 3′ and 5′ overhangs (81). Although fork substrates were efficiently used by nsP2 (Fig. 5*A*), the proposed length of the overhangs at this end of RIs is very short, only 2–3 bases. NsP2 failed to unwind the dsRNA substrate with a considerably longer 6-base 5′ overhang (Fig. 4*B*). Therefore, it is unlikely that these RNA structures are suitable for nsP2 binding in infected cells. Finally, our data indicate that, at least in a test tube reaction, the processivity of nsP2 is relatively low. Taken together, these findings indicate that it is rather unlikely that the role of nsP2 is to unwind long dsRNAs, such as the RIs of alphaviruses. Therefore, a speculative model in which both the RNA helicase and RNA annealing activities of nsP2 may be involved is proposed. According to this model, nsP4 RNA-dependent RNA polymerase functions by adding new nucleotides to the growing positive (genomic or subgenomic) viral RNA, and these RNAs presumably become capped when their synthesis has just been initiated. Therefore, the binding of the nsP2 to the 5′ end of the positive-strand transcript to initiate the capping event leads to this enzyme being situated immediately behind nsP4 where nsP2 may act to separate parental and daughter strands and reanneal parental strands of RIs.

Under the conditions applied here in the analyses of CHIKV helicase functionality, this enzyme was found to be an exclusive RNA helicase. It has been reported previously that the well studied hepatitis C virus NS3 (SF2 helicase) mostly interacts with the phosphodiester backbone of nucleic acids; therefore, it does not discriminate between RNA and DNA substrates (82). Similarly, the SF1 helicase of the severe acute respiratory syndrome coronavirus exhibits enzymatic activities toward both RNA and DNA duplexes (42). Given the significant sequence variability observed in the coding regions of alphaviral nsP2s, it remains to be discovered whether a strict RNA preference is a common property of alphaviral helicases.

In conclusion, in this study, we optimized multiple parameters for the efficient analysis of the NTPase and RNA-modulating properties of CHIKV nsP2 and highlighted the importance of preserving the most native conformation of the enzyme, all of which are important for forthcoming inhibitor screening studies. The establishment of the functional assay to test alphaviral helicase activity and the elaboration of the protocols for the production and purification of biochemically active nsP2 are expected to open avenues for further in-depth structural and functional characterization of this multitalented alphaviral protein.

Acknowledgments—We thank Valeria Lulla for help with manuscript preparation, Margus Rätsep and Jüri Jarvet for help with CD spectroscopy, and Sergo Kasvandik for mass spectrometry analysis.

REFERENCES

1. Burt, F. J., Rolph, M. S., Rulli, N. E., Mahalingam, S., and Heise, M. T. (2012) Chikungunya: a re-emerging virus. *Lancet* **379,** 662–671
2. Strauss, J. H., and Strauss, E. G. (1994) The alphaviruses: gene expression, replication, and evolution. *Microbiol. Rev.* **58,** 491–562
3. Khan, A. H., Morita, K., del Carmen Parquet, M., Hasebe, F., Mathenge, E. G., and Igarashi, A. (2002) Complete nucleotide sequence of chikungunya virus and evidence for an internal polyadenylation site. *J. Gen. Virol.* **83,** 3075–3084
4. Lemm, J. A., Rümenapf, T., Strauss, E. G., Strauss, J. H., and Rice, C. M. (1994) Polypeptide requirements for assembly of functional Sindbis virus replication complexes: a model for the temporal regulation of minus- and plus-strand RNA synthesis. *EMBO J.* **13,** 2925–2934
5. Vasiljeva, L., Merits, A., Golubtsov, A., Sizemskaja, V., Kääriäinen, L., and Ahola, T. (2003) Regulation of the sequential processing of Semliki Forest virus replicase polyprotein. *J. Biol. Chem.* **278,** 41636–41645
6. Lampio, A., Kilpeläinen, I., Pesonen, S., Karhi, K., Auvinen, P., Somerharju, P., and Kääriäinen, L. (2000) Membrane binding mechanism of an RNA virus-capping enzyme. *J. Biol. Chem.* **275,** 37853–37859
7. Mi, S., and Stollar, V. (1991) Expression of Sindbis virus nsP1 and methyltransferase activity in *Escherichia coli*. *Virology* **184,** 423–427
8. Ahola, T., and Kääriäinen, L. (1995) Reaction in alphavirus mRNA capping: formation of a covalent complex of nonstructural protein nsP1 with 7-methyl-GMP. *Proc. Natl. Acad. Sci. U.S.A.* **92,** 507–511
9. Vasiljeva, L., Merits, A., Auvinen, P., and Kääriäinen, L. (2000) Identification of a novel function of the alphavirus capping apparatus. RNA 5′-triphosphatase activity of Nsp2. *J. Biol. Chem.* **275,** 17281–17287
10. Rikkonen, M., Peränen, J., and Kääriäinen, L. (1994) ATPase and GTPase activities associated with Semliki Forest virus nonstructural protein nsP2. *J. Virol.* **68,** 5804–5810
11. Karpe, Y. A., Aher, P. P., and Lole, K. S. (2011) NTPase and 5′-RNA Triphosphatase activities of Chikungunya virus nsP2 protein. *PLoS One* **6,** e22336
12. Hardy, W. R., and Strauss, J. H. (1989) Processing the nonstructural polyproteins of Sindbis virus: nonstructural proteinase is in the C-terminal half of nsP2 and functions both in cis and in trans. *J. Virol.* **63,** 4653–4664
13. Vasiljeva, L., Valmu, L., Kääriäinen, L., and Merits, A. (2001) Site-specific protease activity of the carboxyl-terminal domain of Semliki Forest virus replicase protein nsP2. *J. Biol. Chem.* **276,** 30786–30793
14. Gomez de Cedrón, M., Ehsani, N., Mikkola, M. L., García, J. A., and Kääriäinen, L. (1999) RNA helicase activity of Semliki Forest virus replicase protein NSP2. *FEBS Lett.* **448,** 19–22
15. Malet, H., Coutard, B., Jamal, S., Dutartre, H., Papageorgiou, N., Neuvonen, M., Ahola, T., Forrester, N., Gould, E. A., Lafitte, D., Ferron, F., Lescar, J., Gorbalenya, A. E., de Lamballerie, X., and Canard, B. (2009) The crystal structures of Chikungunya and Venezuelan equine encephalitis virus nsP3 macro domains define a conserved adenosine binding pocket. *J. Virol.* **83,** 6534–6545
16. Shin, G., Yost, S. A., Miller, M. T., Elrod, E. J., Grakoui, A., and Marcotrigiano, J. (2012) Structural and functional insights into alphavirus polyprotein processing and pathogenesis. *Proc. Natl. Acad. Sci. U.S.A.* **109,** 16534–16539
17. Saxton-Shaw, K. D., Ledermann, J. P., Borland, E. M., Stovall, J. L., Mossel, E. C., Singh, A. J., Wilusz, J., and Powers, A. M. (2013) O'nyong nyong virus molecular determinants of unique vector specificity reside in non-structural protein 3. *PLoS Negl. Trop. Dis.* **7,** e1931
18. Rubach, J. K., Wasik, B. R., Rupp, J. C., Kuhn, R. J., Hardy, R. W., and Smith, J. L. (2009) Characterization of purified Sindbis virus nsP4 RNA-dependent RNA polymerase activity *in vitro*. *Virology* **384,** 201–208
19. Peränen, J., Rikkonen, M., Liljeström, P., and Kääriäinen, L. (1990) Nuclear localization of Semliki Forest virus-specific nonstructural protein nsP2. *J. Virol.* **64,** 1888–1896
20. Garmashova, N., Gorchakov, R., Frolova, E., and Frolov, I. (2006) Sindbis virus nonstructural protein nsP2 is cytotoxic and inhibits cellular transcription. *J. Virol.* **80,** 5686–5696
21. Akhrymuk, I., Kulemzin, S. V., and Frolova, E. I. (2012) Evasion of the innate immune response: the Old World alphavirus nsP2 protein induces rapid degradation of Rpb1, a catalytic subunit of RNA polymerase II. *J. Virol.* **86,** 7180–7191
22. Pastorino, B. A., Peyrefitte, C. N., Almeras, L., Grandadam, M., Rolland, D., Tolou, H. J., and Bessaud, M. (2008) Expression and biochemical characterization of nsP2 cysteine protease of Chikungunya virus. *Virus Res.* **131,** 293–298
23. Singleton, M. R., Dillingham, M. S., and Wigley, D. B. (2007) Structure and mechanism of helicases and nucleic acid translocases. *Annu. Rev. Biochem.* **76,** 23–50
24. Gorbalenya, A. E., Koonin, E. V., Donchenko, A. P., and Blinov, V. M. (1989) Two related superfamilies of putative helicases involved in replication, recombination, repair and expression of DNA and RNA genomes. *Nucleic Acids Res.* **17,** 4713–4730
25. Fairman-Williams, M. E., Guenther, U.-P., and Jankowsky, E. (2010) SF1 and SF2 helicases: family matters. *Curr. Opin. Struct. Biol.* **20,** 313–324
26. Subramanya, H. S., Bird, L. E., Brannigan, J. A., and Wigley, D. B. (1996) Crystal structure of a DExx box DNA helicase. *Nature* **384,** 379–383
27. Beran, R. K., Serebrov, V., and Pyle, A. M. (2007) The serine protease domain of hepatitis C viral NS3 activates RNA helicase activity by promoting the binding of RNA substrate. *J. Biol. Chem.* **282,** 34913–34920
28. Chernov, A. V., Shiryaev, S. A., Aleshin, A. E., Ratnikov, B. I., Smith, J. W., Liddington, R. C., and Strongin, A. Y. (2008) The two-component NS2B-NS3 proteinase represses DNA unwinding activity of the West Nile virus NS3 helicase. *J. Biol. Chem.* **283,** 17270–17278
29. Luo, D., Wei, N., Doan, D. N., Paradkar, P. N., Chong, Y., Davidson, A. D., Kotaka, M., Lescar, J., and Vasudevan, S. G. (2010) Flexibility between the protease and helicase domains of the dengue virus NS3 protein conferred by the linker region and its functional implications. *J. Biol. Chem.* **285,** 18817–18827
30. Lulla, A., Lulla, V., and Merits, A. (2012) Macromolecular assembly-driven processing of the 2/3 cleavage site in the alphavirus replicase polyprotein. *J. Virol.* **86,** 553–565
31. Leshchiner, A. D., Solovyev, A. G., Morozov, S. Y., and Kalinina, N. O. (2006) A minimal region in the NTPase/helicase domain of the TGBp1 plant virus movement protein is responsible for ATPase activity and co-

operative RNA binding. *J. Gen. Virol.* **87,** 3087–3095
32. Kelley, L. A., and Sternberg, M. J. (2009) Protein structure prediction on the web: a case study using the Phyre server. *Nat. Protoc.* **4,** 363–371
33. Zhang, Y. (2008) I-TASSER server for protein 3D structure prediction. *BMC Bioinformatics* **9,** 40
34. Eswar, N., Webb, B., Marti-Renom, M. A., Madhusudhan, M. S., Eramian, D., Shen, M.-Y., Pieper, U., and Sali, A. (2007) Comparative protein structure modeling using MODELLER. *Curr. Protoc. Prot. Sci.* **Chapter 2,** Unit 2.9
35. DeLano, W. L. (2002) *The PyMOL Molecular Graphics System*, Version 1.6.0.0, Schrödinger, LLC, New York
36. Lulla, A., Lulla, V., Tints, K., Ahola, T., and Merits, A. (2006) Molecular determinants of substrate specificity for Semliki Forest virus nonstructural protease. *J. Virol.* **80,** 5413–5422
37. Blommel, P. G., and Fox, B. G. (2007) A combined approach to improving large-scale production of tobacco etch virus protease. *Protein Expr. Purif.* **55,** 53–68
38. Golovanov, A. P., Hautbergue, G. M., Wilson, S. A., and Lian, L.-Y. (2004) A simple method for improving protein solubility and long-term stability. *J. Am. Chem. Soc.* **126,** 8933–8939
39. Böhm, G., Muhr, R., and Jaenicke, R. (1992) Quantitative analysis of protein far UV circular dichroism spectra by neural networks. *Protein Eng.* **5,** 191–195
40. Jankowsky, E., and Fairman, M. E. (2008) Duplex unwinding and RNP remodeling with RNA helicases. *Methods Mol. Biol.* **488,** 343–355
41. Karpe, Y. A., and Lole, K. S. (2010) NTPase and 5′ to 3′ RNA duplex-unwinding activities of the hepatitis E virus helicase domain. *J. Virol.* **84,** 3595–3602
42. Adedeji, A. O., Marchand, B., Te Velthuis, A. J., Snijder, E. J., Weiss, S., Eoff, R. L., Singh, K., and Sarafianos, S. G. (2012) Mechanism of nucleic acid unwinding by SARS-CoV helicase. *PLoS One* **7,** e36521
43. Russo, A. T., White, M. A., and Watowich, S. J. (2006) The crystal structure of the Venezuelan equine encephalitis alphavirus nsP2 protease. *Structure* **14,** 1449–1458
44. Nishikiori, M., Sugiyama, S., Xiang, H., Niiyama, M., Ishibashi, K., Inoue, T., Ishikawa, M., Matsumura, H., and Katoh, E. (2012) Crystal structure of the superfamily 1 helicase from tomato mosaic virus. *J. Virol.* **86,** 7565–7576
45. Cheng, Z., Muhlrad, D., Lim, M. K., Parker, R., and Song, H. (2007) Structural and functional insights into the human Upf1 helicase core. *EMBO J.* **26,** 253–264
46. Story, R. M., Weber, I. T., and Steitz, T. A. (1992) The structure of the *E. coli* recA protein monomer and polymer. *Nature* **355,** 318–325
47. Caruthers, J. M., and McKay, D. B. (2002) Helicase structure and mechanism. *Curr. Opin. Struct. Biol.* **12,** 123–133
48. Jankowsky, E., and Fairman-Williams, M. E. (2010) in *RNA Helicases*, RSC Biomolecular Series Vol. 19, pp. 1–31, *Royal Society of Chemistry*, London
49. Shirako, Y., and Strauss, J. H. (1998) Requirement for an aromatic amino acid or histidine at the N terminus of Sindbis virus RNA polymerase. *J. Virol.* **72,** 2310–2315
50. Peroutka, R. J., 3rd, Orcutt, S. J., Strickler, J. E., and Butt, T. R. (2011) SUMO fusion technology for enhanced protein expression and purification in prokaryotes and eukaryotes. *Methods Mol. Biol.* **705,** 15–30
51. Adhikari, S., Manthena, P. V., Sajwan, K., Kota, K. K., and Roy, R. (2010) A unified method for purification of basic proteins. *Anal. Biochem.* **400,** 203–206
52. Waugh, D. S. (2011) An overview of enzymatic reagents for the removal of affinity tags. *Protein Expr. Purif.* **80,** 283–293
53. Gros, C., and Wengler, G. (1996) Identification of an RNA-stimulated NTPase in the predicted helicase sequence of the Rubella virus nonstructural polyprotein. *Virology* **217,** 367–372
54. Lohman, T. M., and Bjornson, K. P. (1996) Mechanisms of helicase-catalyzed DNA unwinding. *Annu. Rev. Biochem.* **65,** 169–214
55. Levin, M. K., Wang, Y.-H., and Patel, S. S. (2004) The functional interaction of the hepatitis C virus helicase molecules is responsible for unwinding processivity. *J. Biol. Chem.* **279,** 26005–26012
56. Lam, A. M., Rypma, R. S., and Frick, D. N. (2004) Enhanced nucleic acid binding to ATP-bound hepatitis C virus NS3 helicase at low pH activates RNA unwinding. *Nucleic Acids Res.* **32,** 4060–4070
57. Gu, M., and Rice, C. M. (2010) Three conformational snapshots of the hepatitis C virus NS3 helicase reveal a ratchet translocation mechanism. *Proc. Natl. Acad. Sci. U.S.A.* **107,** 521–528
58. Taylor, S. D., Solem, A., Kawaoka, J., and Pyle, A. M. (2010) The NPH-II helicase displays efficient DNA x RNA helicase activity and a pronounced purine sequence bias. *J. Biol. Chem.* **285,** 11692–11703
59. Lee, N.-R., Kwon, H.-M., Park, K., Oh, S., Jeong, Y.-J., and Kim, D.-E. (2010) Cooperative translocation enhances the unwinding of duplex DNA by SARS coronavirus helicase nsP13. *Nucleic Acids Res.* **38,** 7626–7636
60. Rajkowitsch, L., Chen, D., Stampfl, S., Semrad, K., Waldsich, C., Mayer, O., Jantsch, M. F., Konrat, R., Bläsi, U., and Schroeder, R. (2007) RNA chaperones, RNA annealers and RNA helicases. *RNA Biol.* **4,** 118–130
61. Yang, Q., and Jankowsky, E. (2005) ATP- and ADP-dependent modulation of RNA unwinding and strand annealing activities by the DEAD-box protein DED1. *Biochemistry* **44,** 13591–13601
62. Frick, D. N., Rypma, R. S., Lam, A. M., and Gu, B. (2004) The nonstructural protein 3 protease/helicase requires an intact protease domain to unwind duplex RNA efficiently. *J. Biol. Chem.* **279,** 1269–1280
63. Gorbalenya, A. E., and Koonin, E. V (1989) Viral proteins containing the purine NTP-binding sequence pattern. *Nucleic Acids Res.* **17,** 8413–8440
64. Yon, C., Teramoto, T., Mueller, N., Phelan, J., Ganesh, V. K., Murthy, K. H., and Padmanabhan, R. (2005) Modulation of the nucleoside triphosphatase/RNA helicase and 5′-RNA triphosphatase activities of Dengue virus type 2 nonstructural protein 3 (NS3) by interaction with NS5, the RNA-dependent RNA polymerase. *J. Biol. Chem.* **280,** 27412–27419
65. Li, H., Clum, S., You, S., Ebner, K. E., and Padmanabhan, R. (1999) The serine protease and RNA-stimulated nucleoside triphosphatase and RNA helicase functional domains of dengue virus type 2 NS3 converge within a region of 20 amino acids. *J. Virol.* **73,** 3108–3116
66. Mayuri, Geders, T. W., Smith, J. L., and Kuhn, R. J. (2008) Role for conserved residues of Sindbis virus nonstructural protein 2 methyltransferase-like domain in regulation of minus-strand synthesis and development of cytopathic infection. *J. Virol.* **82,** 7284–7297
67. Lulla, V., Karo-Astover, L., Rausalu, K., Merits, A., and Lulla, A. (2013) Presentation overrides specificity: probing the plasticity of alphaviral proteolytic activity through mutational analysis. *J. Virol.* **87,** 10207–10220
68. Russo, A. T., Malmstrom, R. D., White, M. A., and Watowich, S. J. (2010) Structural basis for substrate specificity of alphavirus nsP2 proteases. *J. Mol. Graph. Model.* **29,** 46–53
69. Lemm, J. A., and Rice, C. M. (1993) Roles of nonstructural polyproteins and cleavage products in regulating Sindbis virus RNA replication and transcription. *J. Virol.* **67,** 1916–1926
70. Springer, C. L., Huntoon, H. P., and Peersen, O. B. (2013) Polyprotein context regulates the activity of poliovirus 2CATPase bound to bilayer nanodiscs. *J. Virol.* **87,** 5994–6004
71. Rikkonen, M., Peränen, J., and Kääriäinen, L. (1992) Nuclear and nucleolar targeting signals of Semliki Forest virus nonstructural protein nsP2. *Virology* **189,** 462–473
72. Spuul, P., Balistreri, G., Kääriäinen, L., and Ahola, T. (2010) Phosphatidylinositol 3-kinase-, actin-, and microtubule-dependent transport of Semliki Forest virus replication complexes from the plasma membrane to modified lysosomes. *J. Virol.* **84,** 7543–7557
73. Wu, Y. (2012) Unwinding and rewinding: double faces of helicase? *J. Nucleic Acids* **2012,** 140601
74. Pyle, A. M. (2008) Translocation and unwinding mechanisms of RNA and DNA helicases. *Annu. Rev. Biophys.* **37,** 317–336
75. Pyle, A. M. (2011) RNA helicases and remodeling proteins. *Curr. Opin. Chem. Biol.* **15,** 636–642
76. Jankowsky, E. (2011) RNA helicases at work: binding and rearranging. *Trends Biochem. Sci.* **36,** 19–29
77. Rikkonen, M. (1996) Functional significance of the nuclear-targeting and NTP-binding motifs of Semliki Forest virus nonstructural protein nsP2. *Virology* **218,** 352–361
78. Thal, M. A., Wasik, B. R., Posto, J., and Hardy, R. W. (2007) Template requirements for recognition and copying by Sindbis virus RNA-dependent RNA polymerase. *Virology* **358,** 221–232
79. Wengler, G., Wengler, G., and Gross, H. S. (1979) Replicative form of

Semliki Forest virus RNA contains an unpaired guanosine. *Nature* **282,** 754–756
80. Hardy, R. W. (2006) The role of the 3′ terminus of the Sindbis virus genome in minus-strand initiation site selection. *Virology* **345,** 520–531
81. Kulasegaran-Shylini, R., Atasheva, S., Gorenstein, D. G., and Frolov, I. (2009) Structural and functional elements of the promoter encoded by the 5′ untranslated region of the Venezuelan equine encephalitis virus genome. *J. Virol.* **83,** 8327–8339
82. Appleby, T. C., Anderson, R., Fedorova, O., Pyle, A. M., Wang, R., Liu, X., Brendza, K. M., and Somoza, J. R. (2011) Visualizing ATP-dependent RNA translocation by the NS3 helicase from HCV. *J. Mol. Biol.* **405,** 1139–1153